Determination of Ni(II) uptake mechanisms on mordenite surfaces: A combined macroscopic and microscopic approach

S. Yang, G. Sheng, X. Tan, J. Hu, J. Du, Gilles Montavon, X. Wang

Determination of Ni(II) Uptake Mechanisms on Mordenite Surfaces: A Combined Macroscopic and Microscopic Approach

Shitong Yang[1], Guodong Sheng[1], Xiaoli Tan[1], Jun Hu[1], Jinzhou Du[2], Gilles Montavon[3], Xiangke Wang[1]*

1. Key Laboratory of Novel Thin Film Solar Cells, Institute of Plasma Physics, Chinese Academy of Sciences, P.O. Box 1126, Hefei, 230031, P.R. China
2. State Key Laboratory of Estuarine and Coastal Research, East China Normal University, Shanghai, 20062, P.R. China
3. Laboratory SUBATECH, UMR 6457 Ecole des Mines de Nantes/IN2P3-CNRS/Université de Nantes, 4 rue A. Kastler, BP 20722, 44307 Nantes cedex 03, France

*: Corresponding author. Email: xkwang@ipp.ac.cn

Abstract. The uptake mechanisms of Ni(II) on mordenite were investigated by macroscopic experiments and extended X-ray absorption fine structure (EXAFS) spectroscopy. The results demonstrated that Ni(II) could be retained via different mechanisms, depending on pH, ionic strength, temperature etc. At low pH, the uptake of Ni(II) is primarily dominated by cation exchange and/or outer-sphere surface complexation. The interatomic distances of Ni-O (~2.05 Å) and the coordination number (~6.0) are similar to those of Ni(II)(aq) reference sample, suggesting that Ni(II) is present in an $[Ni(H_2O)_6]^{2+}$ octahedral environment at low pH. With increasing pH, the uptake of Ni(II) on mordenite tends to form inner-sphere surface complexes and precipitation/co-precipitation at high pH. The uptake of Ni(II) on

mordenite becomes more favorable with increasing temperature, and the EXAFS spectra analysis show a trend from outer-sphere surface complexation at low temperature to inner-sphere surface complexation at high temperature. The addition of HA/FA increases Ni(II) uptake at low pH and decreases Ni(II) uptake at high pH. Enhanced Ni(II) uptake is attributed to the formation of "ligand-bridging" ternary surface complexes that are adsorbed on mordenite surface, while reduction is attributed to the formation of soluble Ni(II)-HA/FA complexes in solution that compete with uptake processes. The findings presented in this study are important toward a molecular-level description of Ni(II) uptake processes at the water-mineral interface.

1. Introduction

The frequency and severity of heavy metal pollutants in surface and ground water are of great concern to scientists due to the potential hazardous effects on the availability and potability of freshwater sources. Among the potential toxic trace metals, nickel (Ni) is one of the most widespread contaminants in the environment. The wastewater containing Ni mainly derives from industrial production processes such as mining, electrolysis, electroplating, batteries dyes metallurgy, pesticides etc (Parab et al., 2006). Although Ni is relatively non-toxic, elevated levels of Ni are detrimental to the environment. Its presence in drinking water above the permissible limit of 0.02 mg/L set in WHO drinking-water quality standards may directly or indirectly cause adverse health effects such as anemia, encephalopathy, diarrhea, hepatitis, nephritic syndrome,

and the dysfunction of central nervous system. For the sake of ecosystem stability and public health, it is necessary to decrease the concentration of Ni to the permissible limits before its discharge to the environment.

Sorption, diffusion, and precipitation reactions at mineral-water interfaces are closely related with the accumulation, migration, transformation and biological effectiveness of Ni(II) ions in soil and water environment. Zeolites are microporous crystalline solids with well-defined structure, consisting of a three-dimensional network of consisting of silica and alumina tetrahedral units linked by shared oxygen atoms (T-O). The isomorphic substitution of Si^{4+} by Al^{3+} causes a negative charge density in the zeolite lattice. This charge is neutralized by introducing exchanged alkaline and alkaline earth cations (normally Na^{+}, K^{+}, Mg^{2+} and Ca^{2+}) in the structural sites. The mobile non-framework cations are located in cavities in the channel walls and coordinated with the water molecules within the channel. Due to their outstanding properties such as high cation exchange capacity, featuring thermal stability, nanosized pore structures, and unusual surface topology, zeolites are widely used to reduce the heavy metals through chemical immobilization. The treatment process is based either on cation exchange between heavy metals and cations, such as Na^{+}, K^{+}, Mg^{2+} and Ca^{2+}, or on the precipitation of metal hydroxides over the zeolite external surfaces. The uptake kinetics of cation exchange is fast, and exchangeable interlayer cations can be replaced by solute ions by varying the concentration of the hydrated ions. The cation exchange process in zeolites is affected by several factors such as quantity and type of ions, solution pH values and crystal structure of the zeolite. To

67 precisely predict the mobility and long-term behavior of heavy metal ions in zeolite
68 systems, a microscopic mechanistic understanding of metal speciation and chemical
69 processes at the solid-water interface is of fundamental importance.
70 In recent years, X-ray absorption fine structure (XAFS) spectroscopy technique has
71 been widely applied to determine the local atomic structures including interatomic
72 distances, coordination number, and type of near-neighbors surrounding a specific
73 element and oxidation state of the atom. Sano et al. (1987) characterized nickel
74 exchange in Y-type zeolite by EXAFS, and proposed that after NaOH treatment there
75 occurred the formation of nickel hydroxide-type compounds. After oxidation and
76 reduction treatments, metallic nickel particles were formed in the zeolite. Based on
77 the study of cation environment and movement during dehydration and reduction of
78 nickel-exchanged zeolite Y by a combination of EXAFS spectroscopy and XRD
79 technique, Dooryhee et al. (1991) made a conclusion that approximately 70% of the
80 Ni^{2+} present as solvated cations in the supercage were transferred to the hexagonal
81 prism site and stabilized by inward relaxation of the surrounding oxygen ions during
82 dehydration. The remaining Ni^{2+} ions in a partially solvated state in the sodalite cage
83 were readily reducible by hydrogen to yield small crystallites of metallic nickel.
84 Groust et al. (2005) used *in situ* dispersive-EXAFS to identify the oxygen and
85 framework tetrahedral shells around Ni^{2+} in faujasite upon rehydration and found that
86 the Ni^{2+} in fully hydrated $Ni_{2.6}NaX$ were present in an $[Ni(H_2O)_6]^{2+}$ octahedral
87 environment at Ni-O distance of 2.06 Å. In contrast, the Ni-O distance of 2.11 Å in
88 dehydrated $Ni_{2.6}NaX$ is close to a value previously proposed considering that faujasite

is able to accommodate effectively Ni^{2+} at site SI (centre of the hexagonal prism) with six framework O atoms at a bond distance of 2.10 Å (Dooryhee et al., 1991). The above-mentioned literatures thoroughly illustrate the potential of EXAFS to give very specific information on the chemical and/or environmental changes of zeolite catalyst as well as on the migration of nickel in zeolitic systems, even for low loadings of the X-ray absorbing species, thus providing a powerful tool in the fields of catalysis and zeolite science.

Temperature plays a significant role in the dynamic uptake of metal ions, the transformation of surface complexation structures and the stability of various metal precipitates. Scheckel and Sparks (2001) determined the thermodynamics parameters of Ni sorption on pyrophyllite, talc, gibbsite, amorphous silica, and a mixture of gibbsite and amorphous silica over a temperature range of 9 to 35 °C by using the Arrhenius and Eyring equations. Based on the values of E_a (activation energy) and ΔS^0 (standard entropy change), they made a conclusion that the sorption of nickel on these sorbents was surface-controlled and an associative mechanism. The sorption kinetics of Cu and Pb by ferrihydrite was investigated by Scheinost et al. (2001) under two temperatures (6 and 24 °C) that cover a range of common soil and aquifer temperatures. The results showed that the dropping of temperature from 24 to 6 °C reduced both the initial amount of Cu and Pb adsorbed as well as the further sorption kinetics. Besides, temperature had a more pronounced effect on the kinetics of Cu and Pb uptake by ferrihydrite gel than by dense ferrihydrite. Peltier et al. (2006) synthesized a series of Ni-Al LDH phases with NO_3^-, SO_4^{2-} and CO_3^{2-} interlayers by

using a low-temperature controlled hydrolysis method and determined the enthalpies of formation for these phases. The obtained enthalpy and free energies of formation for Ni LDH phases increase in the order of NO_3^- > SO_4^{2-} > CO_3^{2-}. Ni LDH phases are thermodynamically favored over pure Ni hydroxides on minerals containing soluble Al. They also concluded that the substitution of silica for carbonate in the interlayer is a thermodynamically favored process that represents the first step in the transformation of Ni LDHs to phyllosilicate phases with substantially lower Ni solubility than hydroxide phases. Furthermore, the Si-exchanged α-Ni hydroxide is even more stable in thermodynamics than the original Ni-Al LDH (Scheckel et al., 2000). Based on the above-mentioned literatures, the mechanistic and quantitative study of temperature effect on the physicochemical behavior of various metallic surface complexation structures and precipitates can facilitate more accurate predictions of the mobility, toxicity and bioavailability of metal ions in environmental systems.

Humic substances (HS), a kind of natural organic material in soil and natural water bodies, are often intimately associated with natural minerals. HS can form aggregates with minerals by diverse mechanisms such as protonation with formation of hydrogen binding, water and/or metal bridging, ligand exchange and van der Walls interactions (Abate and Masini, 2005). Moreover, the strong complexation ability of HS with metal ions performs a vital function in the environmental fate, bioavailability, toxicity, and mobility of heavy metals in the biosphere. Recently, there has been increased interest in characterizing the mechanisms by which HS and related low molecular

weight organic ligands (e.g., citrate, glutamate) affect metal sorption (Alcacio et al., 2001; Nachtegaal and Sparks, 2003; Strathmann and Myneni, 2004; 2005).

In this study, the uptake of Ni(II) on mordenite as affected by a series of environmental parameters such as pH, ionic strength and temperature in the absence/presence of HS (i.e., humic acid (HA) / fulvic acid (FA)) was investigated by using batch technique under N_2 conditions. The local atomic structures and speciation of the adsorbed Ni(II) on bare and HA/FA-bound mordenite were investigated by using Ni K-edge EXAFS spectra to determine the influence of pH and temperature on the uptake mechanisms.

2. Materials and Methods

2.1 Materials

The mordenite sample was purchased from Nankai University catalyst Co., Ltd (China), and was purified with 1.0 mol/L HNO_3 for 24 h at room temperature to remove the soluble impurity, and then washed with Milli-Q water till to pH ~6.0. At last, the sample was dried in oven at 383.15 K. The crystalline phase of the mordenite was determined by X-ray powder diffraction (XRD). The main peaks and d-spacing values corresponded to pure mordenite by comparing the XRD pattern with that of standard mordenite (Treacy and Higgins, 2001). The Si:Al radio was determined to be ~20:1 by inductively coupled plasma-atomic emission spectrometry (ICP-AES). The cation exchange capacity (CEC) determined by using ammonium acetate method was 91 mmol/100g, and the zero point of charge (pH_{zpc}) measured by potentiometric titration was 4.5. All the other chemicals were purchased in analytical purity and used

without any purification.

Soil HA and FA samples were extracted from the soil of Hua-Jia county (Gansu province, China) and were characterized in detail in earlier studies (Tao et al., 1999; Tan et al., 2008). Cross-polarization magic angle spinning (CPMAS) ^{13}C NMR spectra of HA and FA show that they mainly comprise aliphatic, carbohydrate, aromatic, and carboxyl groups. The concentrations of functional groups of HA and FA determined by fitting the potentiometric acid-base titration data using FITEQL 3.1 are given in Table 1.

2.2 Characterization

The surface groups of mordenite were characterized using FTIR (PerkinElmer Spectrum 100, America) in pressed KBr pellets. The spectral resolution was set to 1 cm^{-1}, and 150 scans were collected for each spectrum. The surface area of mordenite was determined by the Brunauer-Emmett-Teller (BET) method and the pore size distribution was calculated from the sorption branch of the isotherm using the Barrett-Joyner-Halenda (BJH) method. Before determination, the samples were degassed at 423.15 K and 10^{-6} Torr.

2.3 Macroscopic experimental procedure

The macroscopic experiments were carried out in polyethylene tubes under N_2 conditions by using batch technique. The stock suspension of mordenite and $NaClO_4$ solution were first contacted for 24 h to achieve the equilibrium between mordenite and $NaClO_4$. Then, nickel stock solution and HA/FA stock solution were added to achieve the desired concentrations of different components. The solution pH was

adjusted to desired value with negligible amounts of 0.1 or 0.01 mol/L $HClO_4$ or NaOH. The suspensions were gently shaken for 2 days to attain sorption equilibrium, and then the solid was separated from solution by centrifugation at 9000 rpm for 30 min. The concentration of Ni(II) was analyzed by spectrophotometer at wavelength 530 nm through the formation of Ni butanedione dioxime complex. The amount of Ni(II) uptake on mordenite was calculated from the difference between the initial concentration (C_0) and the equilibrium one (C_{eq}) in supernatant. The amount of Ni(II) uptake on mordenite (uptake%=$(C_0-C_{eq})/C_0\times100\%$) and distribution coefficient (K_d=$((C_0-C_{eq})/C_{eq}\cdot V/m)$) were derived from C_0, C_{eq}, the mass of mordenite (m) and the volume of the suspension (V). All experimental data were the average of triplicate determinations and the relative errors were about 5%.

2.4 EXAFS analysis

2.4.1 Sample preparation for EXAFS analysis

Ni(II) uptake samples for EXAFS analysis were conducted using a 250 mL vessel with 0.5 g/L mordenite, 0.01 mol/L $NaClO_4$ and 1.70×10^{-4} mol/L Ni(II) solution under various solution conditions. The uptake of Ni(II) was performed by adding 42.50 mL acidified 0.001 mol/L $Ni(ClO_4)_2$ stock solution and appropriate 0.1 mol/L NaOH to neutralize the acidity of Ni(II) solution. The Ni(II) solution was introduced as follows: 10-50 μL increments of Ni(II) stock solution were introduced into the suspension under constant stirring to disperse the small aliquot of Ni(II) solution, and then the base solution was added. Simultaneously, the pH was monitored and kept to the desired value during Ni(II) addition. Periods of a few minutes between the increments

were chosen to avoid Ni(II)(aq) values exceeding the solubility limit of $Ni(OH)_2(s)$, while allowing the completion of Ni(II) addition in reasonable delay. The samples were shaken for 2 days, and then the samples for EXAFS measurements were prepared from the residual wet pastes obtained after centrifugation of the suspensions.

2.4.2 EXAFS analysis

Ni K-edge X-ray absorption spectra at 8333 eV were recorded at the National Synchrotron Radiation Laboratory (NSRL, Hefei, China) in fluorescence (for Ni(II)(aq), (Ni+HA)(aq), mordenite-Ni and mordenite-HA/FA-Ni) and transmission (for β-$Ni(OH)_2(s)$ and $Ni(CH_3COO)_2{\cdot}4H_2O$) modes. The electron storage ring was operated at 0.8 GeV with a maximum beam current of 200 mA. A superconductor wiggler with a maximum magnetic field B_0 of 6 T inserted in the straight section of the storage ring was used. The energy of X-ray was tuned by using a fixed-exit double-crystal Si (111) monochromator. Higher order harmonics were suppressed by detuning the monochromator by 25%. The monochromator position was calibrated by assigning the first inflection point on the K-absorption edge of metallic nickel foil to 8333.0 eV. Fluorescence spectra were collected using a multi-element pixel high purity Ge solid-state detector. Scans were collected in triplicate and averaged to improve the signal-to-noise ratio. Energy calibration, fluorescence deadtime correction and the EXAFS data analysis were performed with the SixPack interface to the IFEFFIT package. EXAFS data reduction and analyses were performed by using the following procedures. First, the averaged spectra were normalized with respect to E_0 determined from the second derivative of the raw spectra, and then the total atomic

cross-sectional absorption was set to unity. A low-order polynomial function was fit to the pre-edge region and the post-edge region. Next, the data were converted from E-space to *k*-space and weighted by k^3 to compensate for dampening of the XAFS amplitude with increasing *k* space. Fourier transformation was then performed over the *k* range of 2.0-11.0 $Å^{-1}$ using the Kaiser-Bessel window function to obtain the radial structural functions (RSF). Final fitting of the spectra was done on Fourier transformed k^3-weighted spectra in R-space. The theoretical scattering phases and amplitudes used in data analysis were calculated with the scattering code FEFF7 (Ankudinov and Rehr, 1997) using the crystal structure of Ni(II)(aq), β-$Ni(OH)_2$(s) and $Ni(CH_3COO)_2 \cdot 4H_2O$. The amplitude reduction factor, S_0^2, was fixed to 0.85 to reduce the number of adjustable parameters. The need of a unified Debye-Waller factor has been reported to be an effective way for solving the resolution problem and improving the comparability of fitting results. During fitting, the Debye-Waller factors of the Ni-O shells were allowed to vary, but those of the second shells (i.e., Ni-Al/Si/Ni) were fixed equal to that of β-$Ni(OH)_2$(s) (i.e., 0.007 $Å^2$). When allowed to vary, the Debye-Waller factors of the second shells showed no trends for different samples (e.g., as a function of pH and temperature), and therefore the same value of 0.007 $Å^2$ was used in the final fitting procedure to reduce the number of free parameters. This constraint is necessary due to strong correlation of Ni, Al and Si backscattering contributions for the second shells (Mandaliev et al., 2010). On the basis of this fitting mode, we can get more precise and logical results that are helpful to interpret the microscopic uptake mechanisms. Accuracies for R and CN are 0.02 Å

and 20%, respectively, for Ni-O shell and 0.03 Å and 40%, respectively, for the second shells.

3. Results and Discussion

3.1 Characterization of mordenite

The FTIR spectrum of mordenite sample is shown in Fig. 1A. The FTIR bands associated with the internal Si-O(Al) and Si-O(Si) vibrations in tetrahedral or alumino- and silico-oxygen bridges lie in the range of 400-1200 cm^{-1}. The bands relative to the presence of zeolite water lie in the range of 1600-3700 cm^{-1}. From the spectrum, the band at 544 cm^{-1} corresponds to the D_5R (double five ring) structure of tetrahedral SiO_4 and AlO_4 units. The strong band at 1048 cm^{-1} represents the asymmetric valence vibrations in tetrahedra SiO_4 (Korkuna et al., 2006). The less obvious band at 1215 cm^{-1} reflects a low-ordered structure of silicon and aluminum in mordenite crystal. The spectral band at 1637 cm^{-1} reflects the bending H-O-H bond of water molecules retained in the matrix. The broad bands at 3460 and 3608 cm^{-1} are attributed to O-H···O stretching of the water molecules (H_2O) absorbed on the solid surface and the O-H stretching vibration of the silanol (Si-OH) groups from the solid, respectively.

N_2 adsorption-desorption isotherms and the corresponding BJH pore-size distribution curve of the mordenite samples are shown in Fig. 1B. It is clear that the isotherms correspond to Type I classification. The specific surface area and monolayer capacity of the sample are 13.90 m^2/g and 3.19 cm^3/g, respectively. The average pore radius is 5.32 nm with a wide distribution of pore size. The total pore volume is measured to be

0.0370 cm^3/g, including 22.7% micropores (0.0084 cm^3/g) and 77.3% mesopores (0.0286 cm^3/g). It is obvious that mesopores dominate the total pore volume of the sample.

3.2 Macroscopic experiments

3.2.1 Effect of pH and ionic strength

The uptake of Ni(II) on mordenite as a function of pH was measured in 0.001, 0.01 and 0.1 mol/L $NaClO_4$ electrolyte solutions at 293.15 K and the result was shown in Fig. 2A. For pH below 7, the amount of Ni(II) uptake increases gradually with pH increasing and decreases markedly as $NaClO_4$ concentration increases from 0.001 M to 0.1 M. For pH values higher than 7, the uptake of Ni(II) on mordenite increases sharply to a maximum value of ~99%. Above pH 8.5, the uptake of Ni(II) maintains the high level at ~99%. These results imply the changes of uptake mechanisms with pH due to the formation of multifarious surface complexes (Kowal-Fouchard et al., 2004).

It can be seen from Fig. 2A that the uptake of Ni(II) on mordenite is strongly affected by ionic strength at pH<7 and no obvious effect is found at pH>7. The ionic strength can influence the electric double layer thickness and interface potential, thereby can affect the binding of Ni(II) ions. Outer-sphere surface complexes are expected to be more impressionable to ionic strength variations than inner-sphere surface complexes as the background electrolytes are placed in the same plane for outer-sphere surface complexes. It is believed that the uptake mechanism of metal ions is outer-sphere type if an increase in ionic strength results in a decrease of metal ion uptake, while

insensibility to ionic strength has been taken as an indication for inner-sphere surface complexation. Based on the theory mentioned above, one can deduce that cation exchange or outer-sphere surface complexation is the main mechanism for the uptake of Ni(II) on mordenite at pH<7. The fact that the amount of Ni(II) uptake on mordenite decreases as the concentration of $NaClO_4$ increases supports this hypothesis. Fig. 2B shows the relative proportion of Ni(II) species calculated from the hydrolysis constants ($LogK_1$=-9.5, $LogK_2$=-18.0, $LogK_3$=-29.7) (Tertre et al., 2005). It is clear that Ni(II) presents in the forms of Ni^{2+}, $Ni(OH)^{+}$, $Ni(OH)_2$, $Ni(OH)_3^{-}$ and $Ni(OH)_4^{2-}$ at different pH values. One can see that the dominant Ni(II) species is Ni^{2+} at pH<7, and the uptake of Ni(II) in this pH range is mainly accomplished via cation exchange process between Ni^{2+} and H^{+}/Na^{+} that saturates the exchangeable sites. The extent of cation exchange process can be quantified from the exchangeable cationic site concentration and the fraction of Ni(II) species in solution. As mentioned above, the cation exchange capacity (CEC) of mordenite is 91 mmol/100g. Accordingly, the exchangeable cationic site concentration (i.e., H^{+}/Na^{+}) of 0.5 g/L mordenite is 4.55×10^{-4} mol/L, which is 2.7 times of the Ni^{2+} (the dominant Ni(II) species at pH<7) concentration, i.e., 1.70×10^{-4} mol/L. Hence, one can conjecture that the exchange extent should be complete, i.e., one Ni^{2+} replaces two H^{+}/Na^{+} in the structural sites ($2\equiv S-H+Ni^{2+}\rightarrow\equiv S_2-Ni+2H^{+}$ or $2\equiv S-Na+Ni^{2+}\rightarrow\equiv S_2-Ni+2Na^{+}$). In addition to cation exchange, the increase of Ni(II) uptake on mordenite with increasing solution pH may be also attributed to electrostatic action associated with the surface charge of mordenite. At $pH>pH_{zpc}$ (pH_{zpc}=4.5), the surface of mordenite

becomes negatively charged and accordingly enhances the uptake of positively charged Ni^{2+} through electrostatic attraction. Another reason is that the aluminol and silanol groups on mordenite surface are less protonated with pH increasing. Hence, these groups are more available to retain Ni(II) ions. For pH values higher than 7, the effect of $NaClO_4$ concentration on the amount of Ni(II) retained is negligible. The fact is compatible with a more specific process involving hydrolyzed species, in which Ni(II) can associate with mordenite as an inner-sphere complex via covalent bonds between Ni(II) and the electron donating oxygen ions of mordenite surface. Depending on the pH and Ni(II) concentration, the hydrolytic actions of Ni(II) may generate various species such as $Ni(OH)_2$, $Ni(OH)_3^-$ and $Ni(OH)_4^{2-}$ at higher pH values (pH>8.5), which participate in the uptake and precipitation of Ni(II) on mordenite.

From the above discussion, it is clear that the uptake of Ni(II) on mordenite is greatly dependent on solution pH and ionic strength, which implies the combination of various mechanisms such as cation exchange/outer-sphere surface complexes, inner-sphere surface complexes and precipitation. However, the plausible interpretation of the pH-dependent uptake is still controversial and needs further investigation at molecule level, such as the local atomic structures of Ni(II) uptake on mordenite, which is discussed in **Section 3.3.2.1**.

3.2.2 Sorption isotherms and thermodynamic analysis

Figure 3 shows the sorption isotherms of Ni(II) on mordenite at three different temperatures (viz 293.15, 323.15 and 353.15 K). One can see that the uptake of Ni(II)

increases with rise in temperature, which indicates that high temperature is advantageous for Ni(II) uptake on mordenite. Several factors may account for the increase of Ni(II) uptake with increasing temperature. Increased diffusion rate of Ni(II) into the mordenite pores due to increased temperature may account for the observed behavior (Genc-Fuhrman et al., 2004). Changes in the mordenite pore sizes as well as an increase in the number of available surface sites due to the breaking of some internal bonds near mordenite surface edge are expected at higher temperatures. The increase in temperature may lead to the increase in proportion and activity of Ni(II) ions in solution, the affinity of Ni(II) ions to the surface, or the charge and the potential of mordenite surface (Partey et al., 2008).

The thermodynamic parameters ($\Delta H°$, $\Delta S°$, and $\Delta G°$) can be determined from the temperature dependent sorption isotherms. The Gibbs free energy change ($\Delta G°$) is calculated from the relationship:

$$\Delta G^0 = -RTLnK^0 \qquad (1)$$

where $K°$ is the sorption equilibrium constant. Values of $LnK°$, obtained by plotting LnK_d versus C_s for Ni(II) uptake on mordenite and extrapolating C_s to zero, are 9.14 (T=293.15 K), 9.61 (T=323.15 K) and 10.93 (T=353.15 K). Standard entropy change ($\Delta S°$) is calculated using the equation:

$$\Delta S^0 = -\left(\frac{\partial \Delta G^0}{\partial T}\right)_P \qquad (2)$$

The average standard enthalpy change ($\Delta H°$) is then calculated from the relationship:

$$\Delta H^0 = \Delta G^0 + T\Delta S^0 \qquad (3)$$

The values obtained from Eqs. (1) to (3) are tabulated in Table 2. The positive $\Delta H°$

353 values indicate that the uptake process of Ni(II) on mordenite is endothermic. The
354 endothermic nature of Ni(II) uptake is attributed to the disruption of the interfacial
355 water structure and release of water molecules from the surface. At pH 6.5, Ni(II) is in
356 the form of octahedral hydrous Ni(II) ions ($[Ni(H_2O)_6]^{2+}$). The hydration sheath of
357 Ni(II) has to be destroyed before its uptake on mordenite. This dehydration process is
358 essentially an endothermic process, and it appears that the endothermicity of the
359 desolvation process exceeds the exothermicity of Ni(II) ions to attach to mordenite
360 surface by a considerable extent. This implies that structural changes in Ni(II) ions
361 and mordenite units occur during the uptake process. As a result, the number of the
362 water molecules surrounding Ni(II) decreases and thus the degree of the freedom of
363 the water molecules increases. The $\Delta G°$ values for Ni(II) uptake on mordenite at the
364 three temperatures are in the range of -20 to -80 kJ/mol and the uptake of Ni(II) is via
365 physical sorption together with chemisorption (Yu et al., 2001). Moreover, the value
366 of $\Delta G°$ becomes more negative with the increase of temperature, indicating more
367 efficient uptake of Ni(II) at high temperature. The entropy of activation ($\Delta S°$)
368 parameter is generally regarded as a measure of the width of the saddle point of the
369 potential energy surface over which reactant molecules must pass as activated
370 complexes. The large positive $\Delta S°$ values for Ni(II) uptake on mordenite at the three
371 temperatures are in the range of a dissociative mechanism ($\Delta S°$>-10 J/(mol·K)
372 (Scheckel and Sparks, 2001).

373 **3.2.3 Effect of HA and FA**

374 The pH dependent Ni(II) uptake on mordenite in the absence and presence of HA/FA

375 is shown in Fig. 4A. One can see that HA/FA enhances Ni(II) uptake on mordenite at
376 pH<7, while inhibits Ni(II) uptake at pH>7. In general, the uptake of Ni(II) in the
377 presence of HA/FA is explained by a competition between surface complexation
378 (from the mordenite surface and/or adsorbed HA/FA) and non-adsorbed HA/FA in
379 solution. Surface adsorbed HA/FA affect the uptake of Ni(II) by altering surface
380 charges and/or changing available sites for Ni(II) uptake. In the previous literatures
381 (Yan and Bai, 2005; Yang and Xing, 2009), the zeta potentials of HA and FA were
382 determined to be pH ~2. Therefore, at low pH values, the negatively charged HA/FA
383 can be easily adsorbed on the positively charged surfaces of mordenite due to
384 electrostatic attraction. Fig. 4B shows that about 90% HA/FA is adsorbed on
385 mordenite at pH<7, and then the sorption decreases with increasing pH. Actual
386 sorption of HA/FA to mordenite modifies both the long-range electrostatic properties
387 of the aqueous-mordenite interface as well as the concentration and molecular
388 characteristics of specific Ni-binding sites, which results in a more favorable
389 electrostatic environment for Ni(II) uptake and enhances the formation of
390 “ligand-bridging” ternary surface complexes (denoted type B herein) where the Ni(II)
391 ions are complexed by humic molecules that are adsorbed on mordenite surface
392 (Davis, 1984). Humic-promoted Ni(II) uptake is sometimes attributed to a reduction
393 in the net positive surface charge caused by sorption of negatively charged humic
394 molecules, which leads to more favorable electrostatic interactions with dissolved
395 Ni(II) ions. However, at high pH values, the negatively charged HA/FA is difficult to
396 be adsorbed on the negatively charged surfaces of mordenite due to electrostatic

repulsion. The soluble HA/FA forms strong HA/FA-Ni complexes in solution, and thereby competitively diminishes Ni(II) uptake on HA/FA-mordenite hybrids at high pH values (Christl and Kretzschmar, 2001). The result indicates that the complexation ability between HA/FA and Ni(II) is stronger than that between mordenite and Ni(II). In addition to the formation of "ligand-bridging" ternary surface complexes (denoted type B), Ni(II) can also be adsorbed by forming binary Ni(II)-mordenite surface complexes and "metal-bridging" ternary surface complexes (denoted type A herein) (Ali and Dzombak, 1996). The varying contribution of binary and ternary surface complexes to overall Ni(II) uptake at different pH values agrees with expected surface complexation trends.

From Fig. 4A, one can also see that the influence of FA on the uptake of Ni(II) is stronger than that of HA at the whole pH range at the same mass concentrations of FA and HA. Although the HA and FA samples were extracted from the same soil sample and both of them contain functional groups such as hydroxyl, carboxyl, amine and phenolic, the proportions and configurations of these functional groups and surface site densities are different. As illustrated in Table 1, the surface site density of FA (i.e., 2.71×10^{-2} mol/g) is higher than that of HA (i.e., 6.46×10^{-3} mol/g), which means that FA can provide more available surface sites for binding Ni(II). Furthermore, the functional groups of FA such as -OH and -COOH would be ionized as pH increased, leading to the disappearing of these hydrogen-bond donors of FA and the increase of FA solubility (i.e., the decrease of hydrophobic effects) (Yang and Xing, 2009). Therefore, FA has a stronger effect on Ni(II) uptake than HA at the whole pH range.

3.3 EXAFS analysis

3.3.1. EXAFS spectra analysis of reference samples

Figure 5 shows the k^3-weighted spectra and the corresponding Fourier transformed RSFs of the reference samples (Ni(II)(aq), β-$Ni(OH)_2$(s) and $Ni(CH_3COO)_2{\cdot}4H_2O$). One can see that the k^3-weighted spectrum of Ni(II)(aq) (Fig. 5A) exhibits only a single wave frequency of monotonically amplitude for $k > 3Å^{-1}$, which is consistent with the presence of a single ordered coordination sphere. A similar characteristic can be seen in the corresponding RSF (Fig. 5B), which has only a single peak at about 1.6 Å, indicating a single shell of back-scattering O atoms neighboring the central Ni atom. The quantitative analysis shows that Ni is coordinated with ~6 O atoms at interatomic distances of 2.05 Å in Ni(II)(aq) (Table 3), indicating that Ni is in $[Ni(H_2O)_6]^{2+}$ octahedral structures (Dooryhee et al, 1991; Groust et al., 2005). The $[Ni(H_2O)_6]^{2+}$ solution is immediately generated upon dissolution of simple nickel salts in water (Xu et al., 2007). Owing to the contribution of higher shell atoms in the coordination environment of Ni, the k^3-weighted spectra of β-$Ni(OH)_2$(s) and $Ni(CH_3COO)_2{\cdot}4H_2O$ have more distinct structure features than that for Ni(II)(aq). For $Ni(CH_3COO)_2{\cdot}4H_2O$, the RSF spectrum shows an intense peak at 1.6 Å and a small peak between 2.3 and 3.3 Å. Fitting of the first shell peak at 1.6 Å using the theoretically derived phase and amplitude functions indicates the presence of 6 O atoms located at interatomic distances of 2.05 Å. The results are similar to those previously reported for Ni(II) species and are consistent with the NiO_6 octahedron (Scheidegger et al., 1996; Nachtegaal and Sparks, 2003). The spectral intensity

441 between 2.3 and 3.3 Å in the RSF is small and cannot be distinguished from
442 background spectral noise. The second shell spectrum fitting using a single Ni-C
443 proves unsuccessful. For β-$Ni(OH)_2$(s), the Ni-O interatomic distance in the first shell
444 is 2.04 Å with ~6 O atoms, and the Ni-Ni interatomic distance in the second shell is
445 3.11 Å with ~6 Ni atoms (Table 3). The fitting results are consistent with that reported
446 by Scheidegger et al. (1998).

447 **3.3.2 EXAFS analysis of Ni(II) uptake samples**

448 The k^3-weighted spectra and the corresponding Fourier transformed RSFs of all the
449 Ni(II) uptake samples are shown in Figs. 6-8. The EXAFS spectra exhibit distinct
450 changes under various sorption conditions. For the samples prepared at low pH values
451 (i.e., pH 5 and 6.5) and low temperature (293.15 K), the k^3-weighted spectra are
452 dominated by a single sinusoid resulting from O back-scattering in the first shell. The
453 corresponding RSFs of these samples show only a single peak at about 1.6 Å,
454 indicating a single shell of back-scattering O atoms neighboring the central Ni atom.
455 However, additional frequencies appear in the spectra of the other uptake samples,
456 implying the presence of back-scattering from Ni, Al/Si or C in the second
457 coordination shell of the central Ni atom. The data analysis of the Ni-O shell for all
458 the samples are consistent with interatomic distances of ~2.05 Å and coordination
459 number of ~6 O atoms, which reveals that the local atomic structures of Ni-O shell are
460 not influenced by various conditions. Therefore, the EXAFS spectra analyses in the
461 following sections are focused on the coordination environment of the second
462 coordination shell.

463 **3.3.2.1 EXAFS analysis of Ni(II) uptake samples at various pH values**

464 Figure 6 shows the k^3-weighted EXAFS spectra and the corresponding Fourier
465 transformed RSFs for the uptake samples at different pH values. From the k^3-weighted
466 spectra in Fig. 6A, distinct changes can be observed from pH 5.0 to 10.0. At low pH,
467 the spectral noise is more pronounced due to the low Ni loading on the surface. There
468 is a large decrease in the amplitude of the signal at $k > 10$ Å^{-1} as a result of dampening
469 of the EXAFS signal due to a large amount of structure disorder, and the lack of high
470 shell back-scattering in the local atomic structure of the central Ni atom. As pH
471 increases, pronounced features appear in the higher k range at 5 Å^{-1} and 8 Å^{-1}, which
472 are consistent with the presence of heavy back-scattering atoms in the local
473 coordination environment of retained Ni (Dähn et al., 2003; Scheidegger et al., 2000).
474 These features indicate the presence of more than one ordered neighboring shell
475 around Ni atoms, and therefore the outer-sphere surface complexation is not the
476 predominant sorption mode at high pH. In order to isolate the characteristic
477 frequencies that exist in the k^3-weighted spectra, the EXAFS data are Fourier
478 transformed to yield RSFs and the results are shown in Fig. 6B. One can see that all
479 the spectra show a main peak at 1.6 Å, which corresponds to the signal from the first
480 coordination shell of Ni(II). Further peaks are present in the region between 2.3 and
481 3.3 Å. Nevertheless, the intensities are significantly above the background, clearly
482 suggesting the presence of structure beyond the first coordination shell (Sano et al.,
483 1987).

484 A detailed microscopic mechanism of Ni(II) binding to mordenite requires the

485 distinction of different modes of Ni-mordenite phase interaction under various
486 sorption conditions. The EXAFS spectra for the pH-dependent uptake samples may
487 principally include contributions from various Ni(II) species with different
488 coordination environments: Ni adsorbed on the surface of mordenite (formation of
489 outer-sphere or inner-sphere surface complexes) and Ni co-precipitation with fixed
490 and variable stoichiometries. In the case of outer-sphere surface complexation, the
491 hydration sphere and the Ni-O interatomic distances of the surface complex should
492 compare with those of the Ni(aq) reference sample as no direct binding to mordenite
493 surface is anticipated (Duff et al., 2004). By contrast, the Ni complex is directly
494 bonded to the surface via O atoms in the case of inner-sphere surface complexation. In
495 this case, the coordination number of H_2O molecules in the hydration sphere is
496 reduced and the back-scattering contributions from neighboring atoms of mordenite
497 are expected to appear in the EXAFS (Mandaliev et al., 2010). Finally,
498 co-precipitation in solid with fixed and variable stoichiometries at high Ni(II) loadings
499 are a potential mode of Ni(II) immobilization under the high alkaline conditions.
500 The spectra of the samples at pH 5 and 6.5 are successfully fitted with a single layer
501 of hydration, with similar interatomic distances and coordination numbers to those of
502 Ni(II)(aq) reference sample. One can hypothesize that the predominant local atomic
503 structures of the retained Ni is very similar to that of hydrated Ni atoms. As the
504 EXAFS measurement was performed on pastes, the corresponding spectrum signal is
505 heavily weighted toward retained Ni(II) and not aqueous Ni(II) ions. Therefore, the
506 layer of hydration surrounding the central Ni(II) is not disturbed by interactions with

507 the surface. Hence, one can conclude that the uptake of Ni(II) is via cation exchange
508 process between Ni^{2+} and H^{+}/Na^{+} that saturates the exchangeable sites and/or
509 outer-sphere surface complexation in the interlayer space (Strawn and Sparks, 1999;
510 Vasconcelos et al., 2008).
511 With increasing pH, there is increasing deprotonation of AlOH and SiOH sites on the
512 edge of the mordenite particles, although the Si sites are deprotonated at low pH. For
513 the uptake samples at pH 7.5 and 8.0, the extent of Ni(II) uptake has increased relative
514 to that at pH 6.5. The presence of second shell atoms (e.g. Ni/Si/Al) in the RSFs
515 suggests the presence of Ni complexes in these samples. It is not likely that these
516 complexes occur as precipitates since the solution is undersaturated with respect to
517 β-$Ni(OH)_2$(s). Scheidegger et al. (1998) found that Ni can form multinuclear
518 complexes on mineral surfaces even when the solution is undersaturated with respect
519 to the corresponding phase. However, in those studies the second shell metal
520 back-scattering atoms had much larger contributions than the second shell Ni
521 back-scattering contributions in this study. Hence, one can deduce that Ni(II) uptake
522 at pH 7.5 may occur as a mixture of outer-sphere and inner-sphere surface complexes.
523 At pH 8.0, the extent of Ni(II) uptake is increased and is consistent with inner-sphere
524 surface complexation at deprotonated edge sites, although it is likely that some
525 additional Ni(II) is still adsorbed outer-spherically on the basal plane. Based on the
526 deduction mentioned above, the spectra of the two samples prepared at pH 7.5 and 8.0
527 are fitted using Ni-Al/Si pairs (i.e., model 1: Ni-Al, Ni-Si1 and Ni-Si2; model 2:
528 Ni-Al and Ni-Si1; and model 3: Ni-Al and Ni-Si2) and related comparisons are

conducted to obtain the best fit. Our fitting results show that model 1 provides the best fit based on the minimum residual. The results corresponding to this structure model are listed in Table 3. Spectral analysis led to the identification of three nearest cationic subshells containing 1.8 Al at 3.01 Å, 1.7 Si at 3.10 Å and 3.6 Si at 3.27 Å for the uptake sample prepared at pH 7.5, and 2.1 Al at 3.00 Å, 1.8 Si at 3.09 Å and 4.4 Si at 3.28 Å at pH 8.0. The values of interatomic distances are the characteristic of edge-sharing linkages between Ni-Al and Ni-Si1, and of corner-sharing linkages between Ni-Si2 (Dähn et al., 2003). Keeping in mind the fact that some of the second shell distances fall below the separate shells resolution of 0.17 Å that is reported in previous literatures like "EXAFS: Basic principles and data analysis" (Teo, 1986), we determine the statistical relevance of particular parameters in EXAFS fits by using F-test to further check the accuracy and reliability of individual fitting models (Downward et al., 2007). The test results show that fitting based on model 1 yields higher confidence level than models 2 and 3 (data not shown), suggesting the fitting model by using three subshells, i.e., Ni-Al, Ni-Si1 and Ni-Si2 can provide the most reasonable results and help to interpret the microscopic uptake mechanisms under neutral and alkalescence solution conditions.

For the sample prepared at pH 10.0, the k^3-weighted spectrum has some what similar to that of β-$Ni(OH)_2$(s) and the peak at 2.6 Å (dotted line in Fig. 6B) in the corresponding RSF is characteristic of Ni-Ni interaction. The observed precipitate may be attributed to three nucleation products that have been suggested in the previous literatures under similar conditions, i.e., Ni-Al LDH, α-$Ni(OH)_2$ and Ni

551 phyllosilicate (Scheidegger et al., 1998; Thompson et al., 1999; Scheinost et al., 1999;
552 Dähn et al., 2002). The dissolution of an Al-containing sorbent is a prerequisite for the
553 contraction by formation of Ni-Al LDH, and the presence of Si is a prerequisite for
554 the formation of Ni phyllosilicate. The layered single α-$Ni(OH)_2$ is structurally very
555 similar to Ni-Al LDH (Scheinost and Sparks, 2000). To determine the specific
556 contribution of the precipitates to Ni(II) sorption on mordenite, the possible nature of
557 the precipitate is analyzed and discussed. As the mordenite sample contains Al in its
558 constituents, the formation of Ni-Al LDH phases (fit with Ni-Ni and Ni-Al) should be
559 taken into account. The interatomic distances of R_{Ni-Al}=3.30 Å (data not shown)
560 obtained from the numerical simulation is incompatible with synthetic and natural
561 Ni-Al LDH phases (3.03 to 3.07 Å) reported by Thompson et al. (1999). A
562 characteristic beat pattern between 8.0 and 8.5 $Å^{-1}$ in the k^3-weighted spectrum can be
563 used as a fingerprint to unequivocally identify Ni-Al LDHs. Comparison of the Ni-Al
564 LDHs characteristic spectrum (Scheidegger et al., 1997; Dähn et al., 2002) with Ni
565 treated mordenite supports the conclusion that no Ni-Al LDH phase formed under our
566 experimental conditions. To determine whether the formation of $Ni(OH)_2$(s)
567 contributes to Ni(II) uptake on mordenite at pH 10.0, the spectrum of the uptake
568 sample was fitted with two shells (i.e., Ni-O and Ni-Ni). According to this structure
569 model, Ni is surrounded by ~6 neighboring Ni atoms at the interatomic distances of
570 3.07 Å (data not shown). The interatomic distances of 3.07 Å for Ni-Ni shell are close
571 to those of α-$Ni(OH)_2$(s) (Scheinost and Sparks, 2000), suggesting the precipitation of
572 this phase cannot be excluded on the basis of powder EXAFS technique. However,

573 the formation of β-$Ni(OH)_2$(s) (the most stable form of α-$Ni(OH)_2$(s)) can be
574 dismissed as the interatomic distances of Ni-Ni shell in this phase equals 3.12-3.13 Å
575 (Pandya et al., 1990). As the mordenite sample has a high Si:Al radio of ~20:1, the
576 formation of Ni phyllosilicate (fit with Ni-O, Ni-Ni and Ni-Si) for the uptake sample
577 prepared at pH 10.0 are calculated (Table 3). The Ni-Ni and Ni-Si interatomic
578 distances (R_{Ni-Ni} = 3.07 Å and R_{Ni-Si} = 3.27 Å) well match those in Ni phyllosilicates
579 (R_{Ni-Ni} = 3.05 to 3.08 Å, R_{Ni-Si} = 3.26 to 3.27), implying that the nucleation of a Ni
580 phase having a Ni phyllosilicate-like local atomic structure at pH 10.0.

581 **3.3.2.2 EXAFS analysis of Ni(II) uptake samples at different temperatures**

582 In order to gain the microcosmic mechanism of Ni(II) uptake on mordenite at
583 different temperatures, three samples prepared at 293.15, 323.15 and 353.15 K at pH
584 6.5 were selected for EXAFS analysis. The k^3-weighted spectra of the uptake samples
585 at the three temperatures and the corresponding Fourier transformed RSFs are
586 presented in Fig. 7. One can see that the spectra appear distinct and differ from either
587 of the reference samples (Ni(II)(aq) or β-$Ni(OH)_2$(s)). It is clear that the position and
588 amplitude of the first Ni-O peak are relatively constant for the three samples,
589 indicating that the interatomic distances and coordination number of Ni-O shell are
590 not influenced by temperature. However, the intensity of the second Ni-Ni/Si/Al peak
591 increases significantly with temperature rising. In the k^3-weighted spectra (Fig. 7A), a
592 pronounced feature appears at k=5 $Å^{-1}$ for the samples prepared at 323.15 K and
593 353.15 K, which reflects the second coordination shell that is indicative part of
594 inner-sphere surface complexes formed on mordenite surfaces. The EXAFS results

595 reveal that a rise in temperature results in a gain in the inner-sphere surface
596 complexation, which in turn leads to an increase in Ni(II) uptake.
597 The mordenite structure is a framework containing units of 5-member rings of linked
598 SiO_4 and AlO_4 tetrahedra (4 O atoms arranged at the points of a triangular pyramid
599 about a central Si or Al atom). These building units are linked by edge-sharing into
600 chains, which are in turn linked together by 4-rings to form a puckered sheet
601 perforated with 8-ring holes (Meier, 1961). Based on the above-mentioned crystal
602 structure of mordenite, one can deduce that the hydrolyzable Ni could be bound on
603 $Si(Al)O_4$ tetrahedra of mordenite surface via edge-sharing and corner-sharing
604 coordination modes, which are the two most common modes of binding between the
605 polyhedron of hydrated metal ions and the tetrahedron of minerals (Elzinga and
606 Reeder, 2002; Pan et al., 2004). Hence, three subshells, i.e., Ni-Al, Ni-Si1 and Ni-Si2,
607 were used to fit the spectra of the two uptake samples at 323.15 and 353.15 K and a
608 good fit was obtained. The EXAFS analysis results (Table 3) show that the three
609 detectable linkage modes between the adsorbed Ni(II) and the neighboring Al/Si
610 atoms contain 1.9 Al at 3.00 Å, 1.8 Si at 3.10 Å and 3.3 Si at 3.28 Å at T=323.15 K,
611 and 1.8 Al at 3.01 Å, 2.0 Si at 3.09 Å and 4.2 Si at 3.27 Å at T=353.15 K. Again, the
612 spectra fitting residuals and F-test parameters (data not shown) suggest that this model
613 is the most suitable pattern to provide the most reasonable results and help to further
614 interpret the microscopic uptake mechanisms of Ni(II) on mordenite at higher
615 temperatures. Generally, the interatomic distance of edge-sharing linkage is shorter
616 than that of corner-sharing linkage. The short linkage (Ni-Al an Ni-Si1) corresponds

617 to an edge-sharing linkage between the $[Ni(H_2O)_6]^{2+}$ octahedron and the $Si(Al)O_4$
618 tetrahedron, whereas the long linkage (Ni-Si2) reflects the corner-sharing mode (Li et
619 al., 2008). The type of adsorbed Ni(II) has a great influence on the reversibility of
620 adsorbed species. It has been recognized that outer-sphere surface complexation tends
621 to be reversible since they cause minimal changes in the structure of adsorbed species
622 as compared to aqueous species (Scheidegger and Sparks, 1996). Inner-sphere surface
623 complexation reactions tend to be irreversible since they may lead to substantial
624 alterations in the surface structure. The edge linkage (a strong bond) between Ni(II)
625 and mordenite would make it more difficult for Ni(II) to be desorbed from the
626 mordenite surface than the corner linkage (a weak bond) (Elzinga and Reeder, 2002).
627 This implied that the sorption reversibility was influenced not only by the complex
628 type of adsorbed species (i.e., outer-sphere and inner-sphere surface complexes), but
629 more importantly by the proportion of edge-sharing linkage when the two linkage
630 modes existed simultaneously. In a controlled system where Cu(II) sorption on
631 montmorillonite was dominated by edge-sharing linkage, the formation of surface
632 complexes on high-energy edge sites made the sorption rather irreversible (Elzinga
633 and Reeder, 2002). In contrast, the sorption of Zn(II) on δ-MnO_2 was dominated by
634 corner-sharing linkage, which corresponded to a highly reversible sorption (Li et al,
635 2004). Herein, the uptake of Ni(II) on mordenite is between the two extreme cases
636 mentioned above. The EXAFS results (Table 3) indicate that the number of strong
637 sorption (i.e., edge-sharing) sites (CN_{Ni-Al}+CN_{Ni-Si1}) remains relatively stable, while
638 the number of weak sorption (i.e., corner-sharing) sites (CN_{Ni-Si2}) increases as the

639 temperature increases from 323.15 K to 353.15 K. As a result, the ratio of
640 $(CN_{Ni\text{-}Al}+CN_{Ni\text{-}Si1})/CN_{Ni\text{-}Si2}$ drops from 1.12 to 0.90. This observation reveals that the
641 decreased irreversibility at high temperature is attributed to the increase in $CN_{Ni\text{-}Si2}$, or
642 the decrease in the ratio of $(CN_{Ni\text{-}Al}+CN_{Ni\text{-}Si1})/CN_{Ni\text{-}Si2}$ (Pan et al., 2004; Li et al.,
643 2008). On the other hand, the increase in $CN_{Ni\text{-}Si2}$ results in a net increase in overall
644 sorption capacity, which accounts for the observed increase in Ni(II) sorption capacity
645 at high temperature (Fig. 3).

646 **3.3.2.3 EXAFS analysis of Ni(II) uptake samples in the presence of HA/FA**

647 In the presence of 10 mg/L HA/FA, the uptake of Ni(II) on mordenite increases to
648 some extent below pH 7.0, while a slight decrease is observed above pH 7.0 (Fig. 4A).
649 In order to obtain an in-depth microscopic mechanism of the effect of HA/FA on Ni(II)
650 uptake, two samples of Ni(II) uptake in the presence of HA/FA were prepared at pH
651 6.5 for EXAFS analysis. Fig. 8 shows the k^3-weighted spectra and the corresponding
652 Fourier transformed RSFs of the Ni(II)(aq), Ni(II)-HA(aq), Ni(II)-HA-mordenite and
653 Ni(II)-FA-mordenite, which provide evidence for a change in the local atomic
654 structures of Ni(II) when HA/FA is added. For Ni(II)-HA(aq) sample, the spectral
655 intensity between 2.3 and 3.3 Å in the RSF is small and cannot be distinguished from
656 background spectral noise. As a result, no structural information for second shell
657 atoms is provided for the sample, which suggests that Ni(II) is either uncomplexed,
658 complexed via outer-sphere mechanisms (i.e., long-range electrostatic or H-bonding
659 interactions of the carboxylate group of HA with completely solvated Ni(II) ions), or
660 coordinated via a single carboxylate group in a monodentate fashion (i.e., Ni(II)

coordinated to one of the oxygen atoms of the carboxylate group) (Strathmann and Myneni, 2004). The asymmetric features in the k^3-weighted spectra for the Ni(II)-HA-mordenite and Ni(II)-FA-mordenite samples appear no difference from those of Ni(II)(aq) and Ni(II)-HA (aq) solutions. The spectral intensities between 2.3 and 3.3 Å in the RSFs are too small to be distinguished from background spectral noise. This loss in back-scattering intensity indicates that second shell Si/Al atoms are replaced by weak back-scattering atoms such as C from HA/FA molecular, which is supported by the unsuccessful attempt of using a single Ni-Al or Ni-Si back-scattering path or a combination of the two paths to fit the second shell spectrum. Therefore, the dilution of the EXAFS signal from the Ni-Al/Si shell by a Ni-C path is expected. However, second shell spectrum fitting using a single Ni-C also proves unsuccessful. A tentative explanation to the difficulty of obtaining accurate structural information fitting weak Ni-C back-scattering features is that the C atoms in HA/FA molecules are weak back-scattering due to the low atomic number and similar to O atoms, which makes the second shell unconspicuous and therefore prevents a more detailed analysis (Nachtegaal and Sparks, 2003; Strathmann and Myneni, 2005).

4. Ni(II) uptake mechanisms

The macroscopic and microscopic experimental results show that Ni(II) could be retained on mordenite via different mechanisms, depending on various environmental conditions such as pH, ionic strength, temperature etc. At low pH (i.e., pH 5.0 and 6.5) and low temperature (i.e., T=293.15 K), the uptake of Ni(II) is via cation exchange process between Ni^{2+} and H^+/Na^+ that saturates the exchangeable sites and/or

683 outer-sphere surface complexation in the interlayer space (Fig. 9A), which is
684 characterized by less selective and high reversible reactions. The interatomic distance
685 of Ni-O atoms in the first shell for the outer-sphere surface complexes is ~2.05 Å and
686 the coordination number is ~6.0, suggesting that there exists a layer of water
687 molecules between the complexed Ni atoms and the mordenite surface. The extent of
688 Ni(II) uptake at pH 7.5 and 8.0 is increased relative to that at pH 6.5. The presence of
689 second shell atoms (e.g. Al and Si) in the RSFs suggests the presence of inner-sphere
690 surface complexes. Ni(II) uptake at pH 7.5 may occur as a mixture of outer-sphere
691 and inner-sphere surface complexes. At pH 8.0, the extent of Ni(II) uptake is
692 increased and is consistent with inner-sphere surface complexes at deprotonated edge
693 sites (Fig. 9B), which is characterized by more selective and less reversible reactions.
694 The uptake of Ni(II) at pH 10.0 is attributed to the precipitation of α-$Ni(OH)_2$(s)
695 and/or the formation of a Ni phyllosilicate-like co-precipitation (Fig. 9C). The exact
696 contribution between these uptake modes is a function of the speciation of
697 pH-dependent functional groups existing on the surface of mordenite.
698 The EXAFS analysis results of the three temperature-dependent uptake samples
699 demonstrate that Ni(II) can be retained on mordenite surface by forming edge-sharing
700 linkage (strong bond) and corner-sharing linkage (weak bond) simultaneously (Fig.
701 9B). The interatomic distances and corresponding coordination number imply that the
702 observed increase in Ni(II) uptake capacity at high temperature is attributed to the
703 increase of corner-sharing linkage.
704 Addition of HA/FA increases Ni(II) uptake on mordenite at low pH and decreases

Ni(II) uptake at high pH. Enhanced Ni(II) uptake at low pH is attributed to the formation of "ligand-bridging" (type B) ternary surface complexes where Ni(II) ions are complexed by HA/FA molecules that are simultaneously adsorbed to mordenite surfaces. Reductions in Ni(II) uptake at high pH are attributed to the formation of dissolved Ni-HA/FA complexes that compete with uptake processes of Ni(II) on mordenite surface. However, second-shell spectral fits for the Ni-HA/FA-mordenite sorption samples prepared at pH 6.5 using a single Ni-C prove unsuccessful, which may be attributed to that the C atoms in HA/FA molecules are weak back-scattering due to the low atomic number and similar to O atoms.

The attachment of Ni(II) ions specifically bond to mordenite surfaces can severely reduce their bioavailability and mobility in environmental mediums. The findings presented in this study are important toward a molecular-level description of Ni(II) uptake processes at the water-mineral interface. On the other hand, given the restrictions of our experimental conditions, some of the results in this study may have certain limitations in the accuracy of measurement and the discussion of uptake mechanisms. In our further study, we will make great effort to carry out more detailed investigation by using polarized extended X-ray absorption fine structure (P-EXAFS) spectroscopy and other characterization techniques to obtain more precise microstructure information and get more in-depth uptake mechanisms.

Acknowledgements

Authors S.T. Yang and G.D. Sheng contributed equally to this paper. Financial support from National Natural Science Foundation of China (20971126; 20907055; 21077107)

727 and 973 project (2007CB936602; 2011CB933700) from MOST of China are
728 acknowledged. The authors gratefully acknowledge Dr. Bo He and Dr. Fengchun Hu
729 of NSRL, USTC for helpful technical assistance of EXAFS experiments. We also
730 thank Prof. B. Grambow (SUBATECH, France) for favorable discussion to improve
731 the quality of the manuscript.

732 **References**

733 Abate G. and Masini J.C. (2005) Influence of pH, ionic strength and humic acid on
734 adsorption of Cd(II) and Pb(II) onto vermiculite. Colloid Surf. A 262, 33-39.

735 Alcacio T. E., Hesterberg D., Chou J.W., Martin J. D., Beauchemin S. and Sayers D.E.
736 (2001) Molecular scale characteristics of Cu(II) bonding in goethite humate
737 complexes. Geochim. Cosmochim. Acta 65, 1355-1366.

738 Ali M.A. and Dzombak D.A. (1996) Effects of simple organic acids on sorption of
739 Cu^{2+} and Ca^{2+} on goethite. Geochim. Cosmochim. Acta 60, 291-304.

740 Ankudinov A.L. and Rehr J.J. (1997) Relativistic calculations of spin-dependent
741 x-ray-absorption spectra. Phys. Rev. B 56, 1712-1715.

742 Christl I. and Kretzschmar R. (2001) Interaction of copper and fulvic acid at the
743 hematite-water interface. Geochim. Cosmochim. Acta 65, 3435-3442.

744 Dähn, R., Scheidegger A.M., Manceau A., Schlegel M.L., Baeyens B., Bradbury M.H.
745 and Morales M. (2002) Neoformation of Ni phyllosilicate upon Ni uptake on
746 montmorillonite: a kinetics study by powder and polarized extended X-ray
747 absorption fine structure spectroscopy. Geochim. Cosmochim. Acta 66,
748 2335-2347.

749 Dähn R., Scheidegger A.M., Manceau A., Schlegel M.L., Baeyens B., Bradbury, M.H.
750 and Chateigner D. (2003) Structural evidence for the sorption of Ni(II) atoms on
751 the edges of montmorillonite clay minerals: a polarized X-ray absorption fine
752 structure study. Geochim. Cosmochim. Acta 67, 1-15.
753 Davis, J.A. (1984) Complexation of trace metals by adsorbed natural organic matter.
754 Geochim. Cosmochim. Acta 48, 679-691.
755 Dooryhee E., Catlow C.R.A., Couves J.W., Maddox P.J. and Thomas J.M. (1991) A
756 study of cation environment and movement during dehydration and reduction of
757 nickel-exchanged zeolite Y by x-ray absorption and diffraction. J. Phys. Chem.
758 95, 4514-4521.
759 Downward L., Booth C.H., Lukens W.W. and Bridges F. (2007) A Variation of the
760 F-Test for determining statistical relevance of particular parameters in EXAFS
761 fits. AIP Conference Proceedings 882, 129-131.
762 Duff M.C., Hunter D.B., Hobbs D.T., Fink S.D., Dai Z. and Bradley J.P. (2004)
763 Mechanisms of strontium and uranium removal from high-level radioactive
764 waste simulant solutions by the sorbent monosodium titanate. Environ. Sci.
765 Technol. 38, 5200-5207.
766 Elzinga E.J. and Reeder R.J. (2002) X-ray absorption spectroscopy study of Cu^{2+} and
767 Zn^{2+} adsorption complexes at the calcite surface: Implications for site-specific
768 metal incorporation preferences during calcite crystal growth. Geochim.
769 Cosmochim. Acta 66, 3943-3954.
770 Genc-Fuhrman H., Tjell J.C. and McConchie D. (2004) Adsorption of arsenic from

771 water using activated neutralized red mud. Environ. Sci. Technol. 38, 2428-2434.
772 Groust J.F., Pommier C., Stievano L., Villain F., Giorgetti C., Baudelet F. and
773 Massiani P. (2005) Real time monitoring of the evolution of Ni^{2+} environment in
774 faujasite upon rehydration by *in situ* dispersive-EXAFS. Catal. Lett. 102,
775 257-260.
776 Korkuna O., Leboda R., Skubiszewska-Zięba J., Vrublevs'ka T., Gun'ko V.M. and
777 Ryczkowski J. (2006) Structural and physicochemical properties of natural
778 zeolites: clinoptilolite and mordenite. Microp. Mesop. Mater. 87, 243-254.
779 Kowal-Fouchard A., Drot R., Simoni E. and Ehrhardt J.J. (2004) Use of spectroscopic
780 techniques for uranium(VI)/montmorillonite interaction modeling. Environ. Sci.
781 Technol. 38, 1399-1407.
782 Li W., Pan G., Zhang M., Zhao D., Yang Y., Chen H. and He G. (2008) EXAFS studies
783 on adsorption irreversibility of Zn(II) on TiO_2: temperature dependence. J.
784 Colloid Interf. Sci. 319, 385-391.
785 Li X.L., Pan G., Qin Y.W., Hu T.D., Wu Z.Y. and Xie Y.N. (2004) EXAFS studies on
786 adsorption-desorption reversibility at manganese oxide-water interfaces II.
787 Reversible adsorption of zinc on δ-MnO_2. J. Colloid Interf. Sci. 271, 35-40.
788 Mandaliev P., Dähn R., Tits J., Wehrli B. and Wieland E. (2010) EXAFS study of
789 Nd(III) uptake by amorphous calcium silicate hydrates (C-S-H). J. Colloid Interf.
790 Sci. 342, 1-7.
791 Meier W.M. (1961) The crystal structure of mordenite (ptilolite). Z. Kristallogr. 115,
792 439-450.

793 Nachtegaal M. and Sparks D. L. (2003) Nickel sequestration in a kaolinite-humic acid
794 complex. Environ. Sci. Technol. 37, 529-534.
795 Pandya K.I., O'Grady W.E., Corrigan D.A., McBreen J. and Hoffman R.W. (1990)
796 Extended x-ray absorption fine structure investigation of nickel hydroxides. J.
797 Phys. Chem. 94, 21-26.
798 Pan G., Qin Y.W., Li X.L., Hu T.D., Wu Z.Y. and Xie Y.N. (2004) EXAFS studies on
799 adsorption-desorption reversibility at manganese oxides-water interfaces I.
800 Irreversible adsorption of zinc onto manganite (γ-MnOOH). J. Colloid Interf.
801 Sci. 271, 28-34.
802 Parab H., Joshi S., Shenoy N., Lali A., Sarma U.S. and Sudersanan M. (2006)
803 Determination of kinetic and equilibrium parameters of the batch adsorption of
804 Co(II), Cr(III) and Ni(II) onto coir pith. Process Biochem. 41, 609-615.
805 Partey F., Norman D., Ndur S. and Nartey R. (2008) Arsenic sorption onto laterite
806 iron concretions: temperature effect. J. Colloid Interf. Sci. 321, 493–500.
807 Peltier E., Allada R., Navrotsky A. and Sparks D.L. (2006) Nickel solubility and
808 precipitation in soils: a thermodynamic study. Clay Clay Miner. 54, 153-164,
809 Sano M., Maruo T., Yamatera H., Suzuki M. and Saito Y. (1987) EXAFS studies on
810 the origin of highly catalytic activity in nickel Y zeolite. J. Am. Chem. SOC. 109,
811 52-55.
812 Scheckel K.G., Scheinost A.C., Ford R.G. and Sparks D.L. (2000) Stability of layered
813 Ni hydroxide surface precipitates-a dissolution kinetics study. Geochim.
814 Cosmochim. Acta 64, 2727-2735.

Scheckel K.G. and Sparks D.L. (2001) Temperature effects on nickel sorption kinetics at the mineral-water interface. Soil Sci. Soc. Am. J. 65, 719-728.

Scheidegger A.M. and Sparks D.L. (1996) A critical assessment of sorption-desorption mechanisms at the soil mineral/water interface. Soil Sci. 161, 813-831.

Scheidegger A.M., Lamble G.M. and Sparks D.L. (1996) Investigation of Ni sorption on pyrophyllite: An XAFS study. Environ. Sci. Technol. 30, 548-554.

Scheidegger A.M., Lamble G.M. and Sparks D.L. (1997) Spectroscopic evidence for the formation of mixed-cation hydroxide phases upon metal sorption on clays and aluminum oxides. J. Colloid Interf. Sci. 186, 118-128.

Scheidegger A.M., Strawn D.G., Lamble G.M. and Sparks D. L. (1998) The kinetics of mixed Ni-Al hydroxide formation on clay and aluminum oxide minerals: a time-resolved XAFS study. Geochim. Cosmochim. Acta 62, 2233-2245.

Scheidegger A.M., Wieland E., Scheinost A.C., Dähn R. and Spieler P. (2000) Spectroscopic evidence for the formation of layered Ni-Al double hydroxides in cement. Environ. Sci. Technol. 34, 4545-4548.

Scheinost A.C., Ford R.G. and Sparks D.L. (1999) The role of Al in the formation of secondary Ni precipitates on pyrophyllite, gibbsite, talc, and amorphous silica: A DRS study. Geochim. Cosmochim. Acta 63, 3193-3203.

Scheinost A.C., Abend S., Pandya K.I. and Sparks D.L. (2001) Kinetic controls on Cu and Pb sorption by ferrihydrite. Environ. Sci. Technol. 35, 1090-1096.

Scheinost A.C. and Sparks D.L. (2000) Formation of layered single- and double-metal

837 hydroxide precipitates at the mineral/water interface: a multiple-scattering XAFS
838 analysis. J. Colloid Interf. Sci. 223, 167-178.
839 Strathmann T.J. and Myneni S.C.B. (2004) Speciation of aqueous Ni(II)-carboxylate
840 and Ni(II)-fulvic acid solutions: combined ATR-FTIR and XAFS analysis.
841 Geochim. Cosmochim. Acta 68, 3441-3458.
842 Strathmann T.J. and Myneni S.C.B. (2005) Effect of soil fulvic acid on nickel(II)
843 sorption and bonding at the aqueous-boehmite (γ-AlOOH) interface. Environ. Sci.
844 Technol. 39, 4027-4034.
845 Strawn D.G. and Sparks D.L. (1999) The use of XAFS to distinguish between inner-
846 and outer-sphere lead adsorption complexes on montmorillonite. J. Colloid Interf.
847 Sci. 216, 257-269.
848 Tan X.L., Wang X.K., Geckeis H. and Rabung T. (2008) Sorption of Eu(III) on humic
849 acid or fulvic acid bound to alumina studied by SEM-EDS, XPS, TRLFS and
850 batch techniques. Environ. Sci. Technol. 42, 6532-6537.
851 Tao Z.Y., Zhang J. and Zhai J. (1999) Characterization and differentiation of humic
852 acids and fulvic acids in soils fromvarious regions of China by nuclearmagnetic
853 resonance spectroscopy. Anal. Chim. Acta 395, 199-203.
854 Teo B.K. (1986) EXAFS: Basic principles and data analysis. Springer-Verlag (Berlin
855 and New York) 9, pp1-349.
856 Tertre E., Berger G., Castet S., Loubet M. and Giffaut E. (2005) Experimental sorption
857 of Ni^{2+},Cs^{+} and Ln^{3+} onto a montmorillonite up to 150°C. Geochim. Cosmochim.
858 Acta 69, 4937-4948.

859 Thompson H.A., Parks G.A. and Brown Jr. G.E. (1999) Ambient-temperature
860 synthesis, evolution, and characterization of cobalt–aluminum hydrotalcite-like
861 solids. Clays Clay Miner. 47, 425-438.
862 Treacy M.M.J. and Higgins J.B. (2001) Collection of simulated XRD powder patterns
863 for zeolites, in: Published on behalf of the structure commission of the
864 international zeolite association, fourth revised edition, Elsevier.
865 (<http://www.iza-structure.org/databases>).
866 Vasconcelos I.F., Haack E.A., Maurice P.A. and Bunker B.A. (2008) EXAFS analysis
867 of cadmium(II) adsorption to kaolinite. Chem. Geol. 249, 237-249.
868 Xu Y., Axe L., Boonfueng T., Tyson T.A., Trivedi P. and Pandya K. (2007) Ni(II)
869 complexation to amorphous ferric oxide: an X-ray absorption spectroscopy study.
870 J. Colloid Interf. Sci. 314, 10-17.
871 Yan W.L. and Bai R.B. (2005) Adsorption of lead and humic acid on chitosan
872 hydrogel beads. Water Res. 39, 688-698.
873 Yang K. and Xing B.S. (2009) Adsorption of fulvic acid by carbon nanotubes from
874 water. Environ. Pollut. 157, 1095-1100.
875 Yu Y., Zhuang Y.Y. and Wang Z.H. (2001) Adsorption of water-soluble dye onto
876 functionalized resin. J. Colloid Interf. Sci. 242, 288-293.
877

878 Table 1. The concentrations of functional groups of HA and FA calculated from
879 potentiometric titration by using FITEQL 3.1.

	Log K_a			C (mol/g)*			Surface sites density (mol/g)	WSOS/DF
	L_1	L_2	L_3	HL_1	HL_2	HL_3		
HA	-5.04	-7.40	-9.60	2.20×10^{-3}	1.08×10^{-3}	3.18×10^{-3}	6.46×10^{-3}	2.37
FA	-5.19	-7.77	-10.53	1.83×10^{-3}	1.08×10^{-3}	2.42×10^{-2}	2.71×10^{-2}	0.10

*: HL_1, HL_2 and HL_3 represent the carboxyl groups (-COOH), the phenolic groups (Ar-OH) and the amine groups ($-NH_2$) of HA and FA, respectively.

880

881 Table 2. Values of thermodynamic parameters for the uptake of Ni(II) on Mordenite.

T(K)	Δ*G*° (kJ/mol)	Δ*S*° (J/(mol·K))	Δ*H*° (kJ/mol)
293.15	-22.27	163.50	25.66
323.15	-25.81	163.50	27.02
353.15	-32.08	163.50	25.67

882

883 Table 3. Structural Parameters Derived from EXAFS Analysis for Standard
884 References and Ni uptake samples.

Sample Conditions	First shell (Ni-O)			Second shell (Ni-Ni/Al/Si)				% Res
	R (Å)	CN	σ^2 (Å^2)	Bond	R (Å)	CN	σ^2 (Å^2)	
Ni(II)(aq)	2.05(1)	5.9(2)	0.004(1)					4.2
β-$Ni(OH)_2$	2.04(2)	5.8(1)	0.005(1)	Ni-Ni	3.11(1)	6.0(1)	0.007	6.8
$Ni(CH_3COO)_2 \cdot 4H_2O$	2.05(1)	6.0(2)	0.003(2)					5.2
(Ni(II)+HA)(aq)	2.03(2)	6.0(3)	0.004(1)					5.8
pH 5.0, 293.15K	2.05(1)	6.1(1)	0.004(2)					4.5
pH 6.5, 293.15K	2.04(2)	5.9(2)	0.005(2)					4.9
pH 7.5, 293.15K	2.04(1)	5.6(2)	0.004(1)	Ni-Al	3.01(3)	1.8(4)	0.007	9.9
				Ni-Si1	3.10(2)	1.7(3)	0.007	
				Ni-Si2	3.27(2)	3.6(6)	0.007	
pH 8.0, 293.15K	2.03(1)	5.8(1)	0.003(2)	Ni-Al	3.00(3)	2.1(4)	0.007	8.9
				Ni-Si1	3.09(1)	1.8(5)	0.007	
				Ni-Si2	3.28(2)	4.4(3)	0.007	
pH 10.0, 293.15K	2.03(2)	5.8(1)	0.004(1)	Ni-Ni	3.07(2)	2.1(2)	0.007	10.4
				Ni-Si	3.27(2)	3.2(3)	0.007	
pH 6.5, 323.15K	2.04(1)	5.7(2)	0.004(2)	Ni-Al	3.00(3)	1.9(3)	0.007	10.2
				Ni-Si1	3.10(3)	1.8(4)	0.007	
				Ni-Si2	3.28(3)	3.3(6)	0.007	
pH 6.5, 353.15K	2.03(2)	5.8(1)	0.005(1)	Ni-Al	3.01(3)	1.8(3)	0.007	9.3
				Ni-Si1	3.09(2)	2.0(3)	0.007	
				Ni-Si2	3.27(3)	4.2(4)	0.007	
pH 6.5, 10 mg/L HA	2.05(1)	5.9(2)	0.005(1)					6.9
pH 6.5, 10 mg/L FA	2.04(2)	5.8(1)	0.004(2)					7.6

R--Interatomic distance, CN--Coordination number, σ^2--Debye-Waller factor, Res--a measure of the agreement between experimental and theoretical EXAFS curves. Debye-Waller factors for all the second-shell fits were constrained to remain equal during the data analysis. Ni(II)(aq), β-$Ni(OH)_2$ and $Ni(CH_3COO)_2 \cdot 4H_2O$ are named as reference samples, and the other samples of mordenite with retained Ni(II) are named as uptake samples.

885
886
887
888
889
890

Figure Captions

Fig. 1 FTIR spectrum (A) and N_2 adsorption-desorption isotherms of mordenite sample (B).

Fig. 2 Effect of pH and ionic strength on Ni(II) uptake on mordenite (A) and the relative proportion of Ni(II) species at various pH values (B). T=293.15 K, m/V= 0.5 g/L, $C_{Ni(II)initial}$=1.70×10^{-4} mol/L.

Fig. 3 Sorption isotherms of Ni(II) on mordenite at three different temperatures. pH=6.5, m/V=0.5g/L, $C_{Ni(II)initial}$= 3.41×10^{-5}~3.41×10^{-4} mol/L, I=0.01 mol/L $NaClO_4$.

Fig. 4 Effect of HA/FA on Ni(II) uptake on mordenite as a function of pH (A) and HA/FA sorption on mordenite as a function of pH. T=293.15 K, m/V=0.5 g/L, $C_{Ni(II)initial}$=1.70×10^{-4} mol/L, $C_{HA/FA}$=10 mg/L, I=0.01 mol/L $NaClO_4$.

Fig. 5 k^3-weighted spectra (A) and Radial structure functions (RSFs) (B) produced by forward Fourier transforms (uncorrected for phase shift) of reference samples. Solid and dash lines represent experimental spectra and spectral fits, respectively.

Fig. 6 k^3-weighted spectra (A) and Radial structure functions (RSFs) (B) produced by forward Fourier transforms (uncorrected for phase shift) of Ni uptake on mordenite at various pH values. Solid and dash lines represent experimental spectra and spectral fits, respectively. m/V=0.5 g/L, pH=5.0, 6.5, 7.5, 8.0 and 10.0, $C_{Ni(II)initial}$=1.70×10^{-4} mol/L, T=293.15 K, I=0.01 mol/L $NaClO_4$.

Fig. 7 k^3-weighted spectra (A) and Radial structure functions (RSFs) (B) produced by forward Fourier transforms (uncorrected for phase shift) of Ni uptake on mordenite at various temperatures. Solid and dash lines represent experimental spectra and spectral

fits, respectively. m/V=0.5 g/L, pH=6.5, $C_{Ni(II)initial}$=1.70×10^{-4} mol/L, T=293.15, 323.15 and 353.15 K, I=0.01 mol/L $NaClO_4$.

Fig. 8 k^3-weighted spectra (A) and Radial structure functions (RSFs) (B) produced by forward Fourier transforms (uncorrected for phase shift) of Ni uptake on mordenite in the presence of HA/FA. Solid and dash lines represent experimental spectra and spectral fits, respectively. m/V=0.5 g/L, pH=6.5, $C_{Ni(II)initial}$=1.70×10^{-4} mol/L, $C_{HA/FA}$=10 mg/L, T=293.15 K, I=0.01 mol/L $NaClO_4$.

Fig. 9 Schematic presentation of the possible mechanisms of Ni(II) interaction with mordenite phases: (A) Cation exchange/Outer-sphere surface complexation; (B) Inner-sphere surface complexation; (C) Precipitation/Co-precipitation.

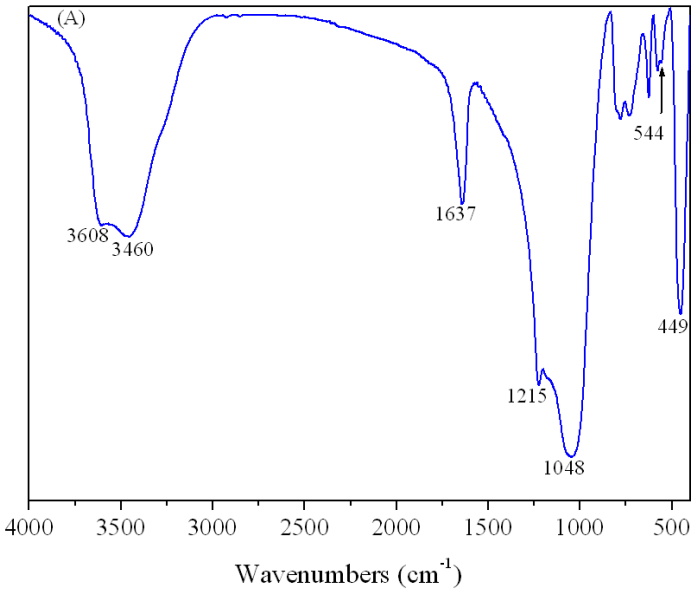
(A)
3608
3460
1637
1215
1048
544
449
4000
3500
3000
2500
2000
1500
1000
500
Wavenumbers (cm-1)

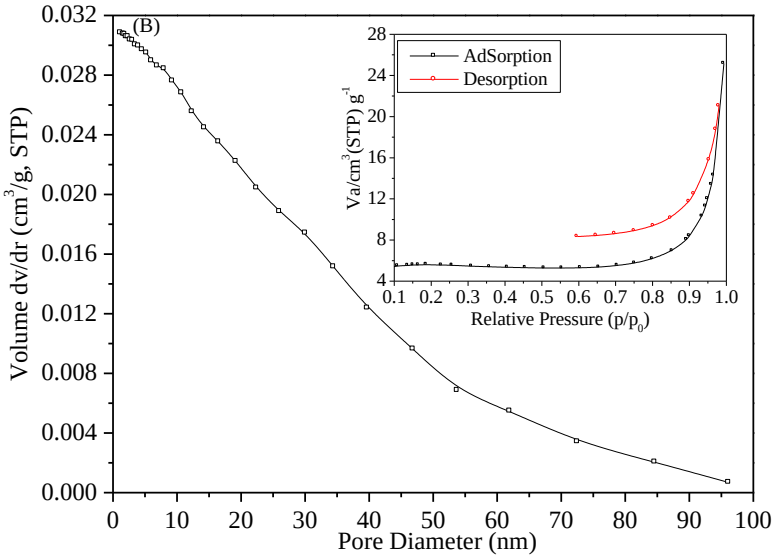
(B)
Volume dv/dr (cm3/g, STP)
Pore Diameter (nm)
AdSorption
Desorption
Va/cm3(STP) g-1
Relative Pressure (p/p0)

Fig. 1

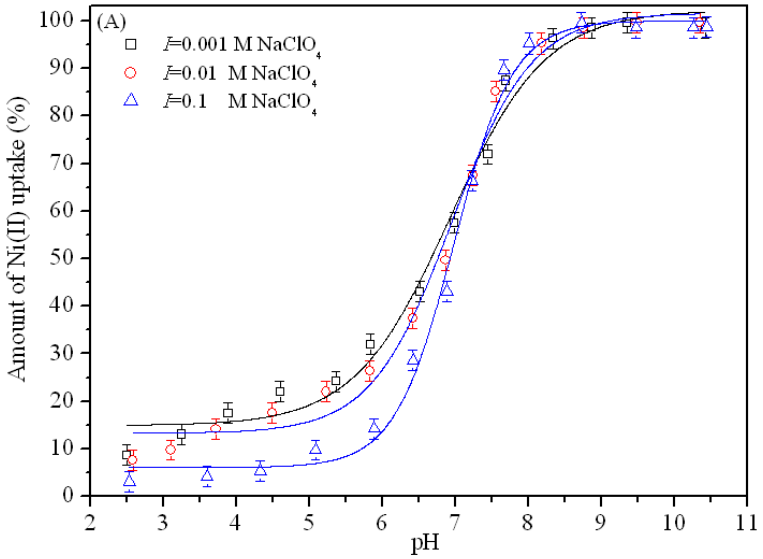

939

940

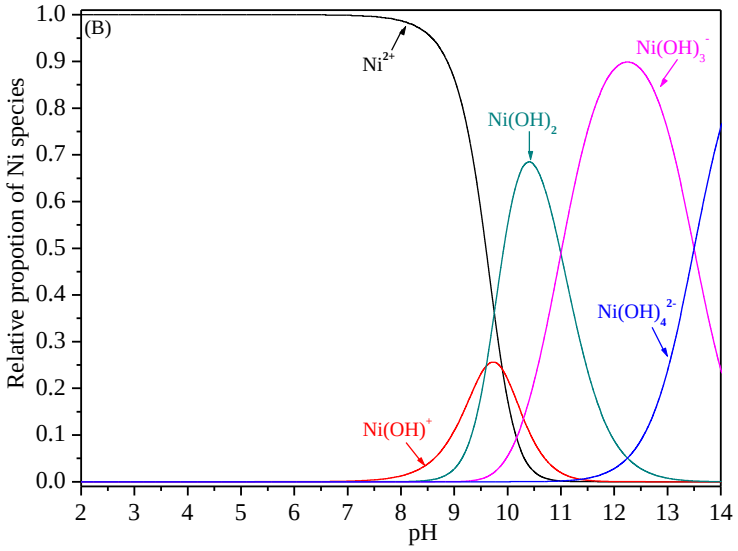

941

942 Fig. 2

943

944

945

946

947

948

949

950

951

952

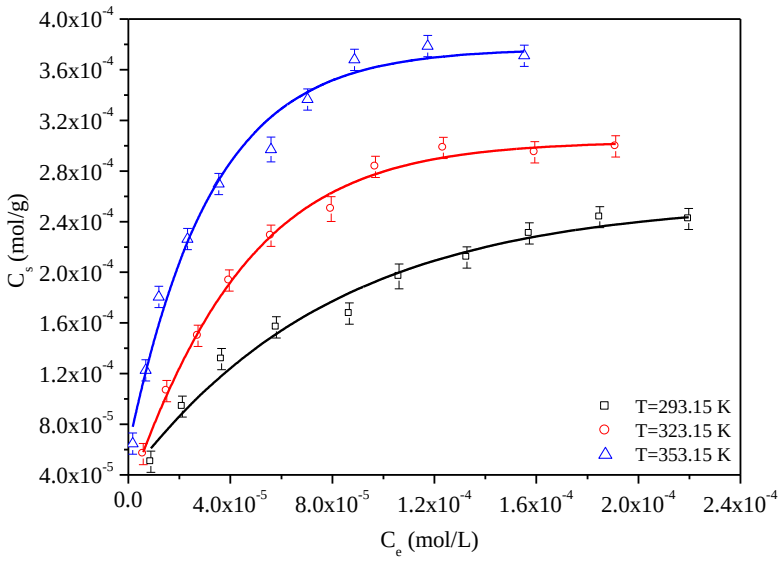
4.0x10-4
3.6x10-4
3.2x10-4
2.8x10-4
2.4x10-4
2.0x10-4
1.6x10-4
1.2x10-4
8.0x10-5
4.0x10-5
Cs (mol/g)
0.0
4.0x10-5
8.0x10-5
1.2x10-4
1.6x10-4
2.0x10-4
2.4x10-4
Ce (mol/L)
T=293.15 K
T=323.15 K
T=353.15 K

Fig. 3

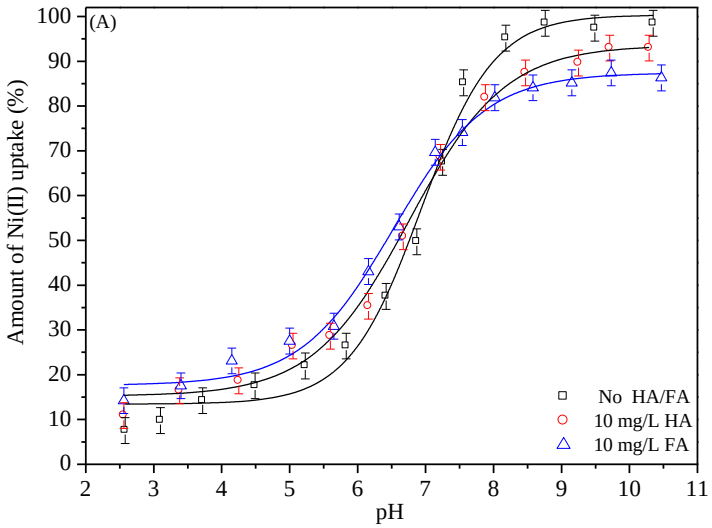

968

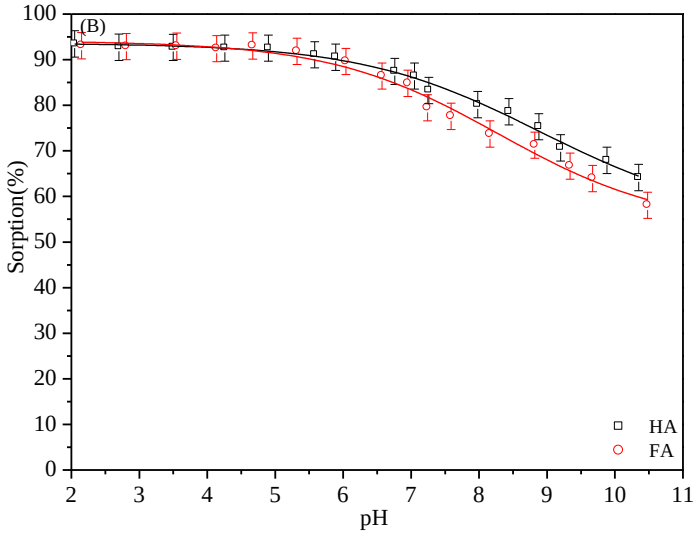

969

970 Fig. 4

971

972

973

974

975

976

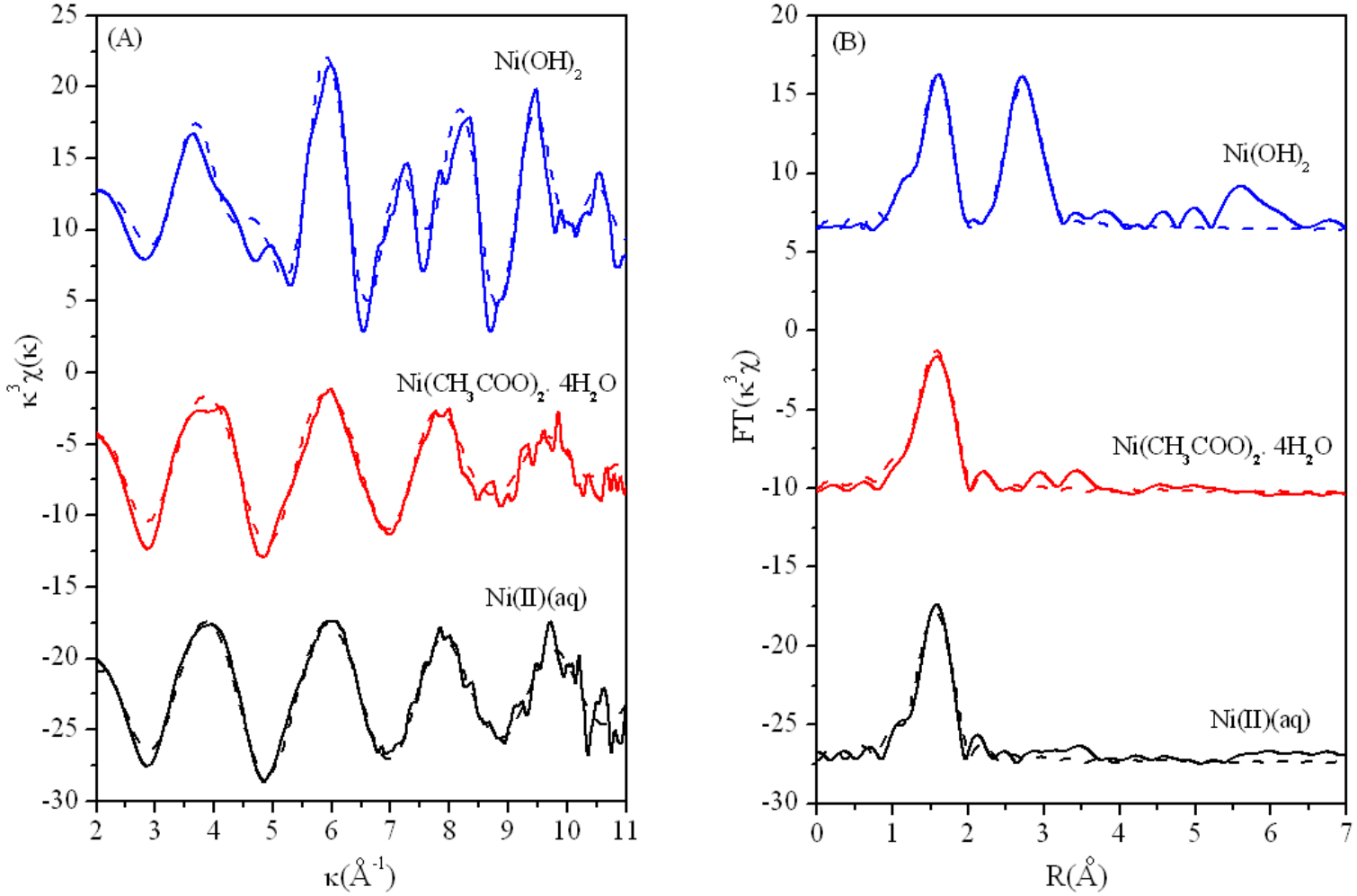
(A)
Ni(OH)2
Ni(CH3COO)2. 4H2O
Ni(II)(aq)
κ3χ(κ)
κ(Å-1)
(B)
Ni(OH)2
Ni(CH3COO)2. 4H2O
Ni(II)(aq)
FT(κ3χ)
R(Å)

Fig. 5

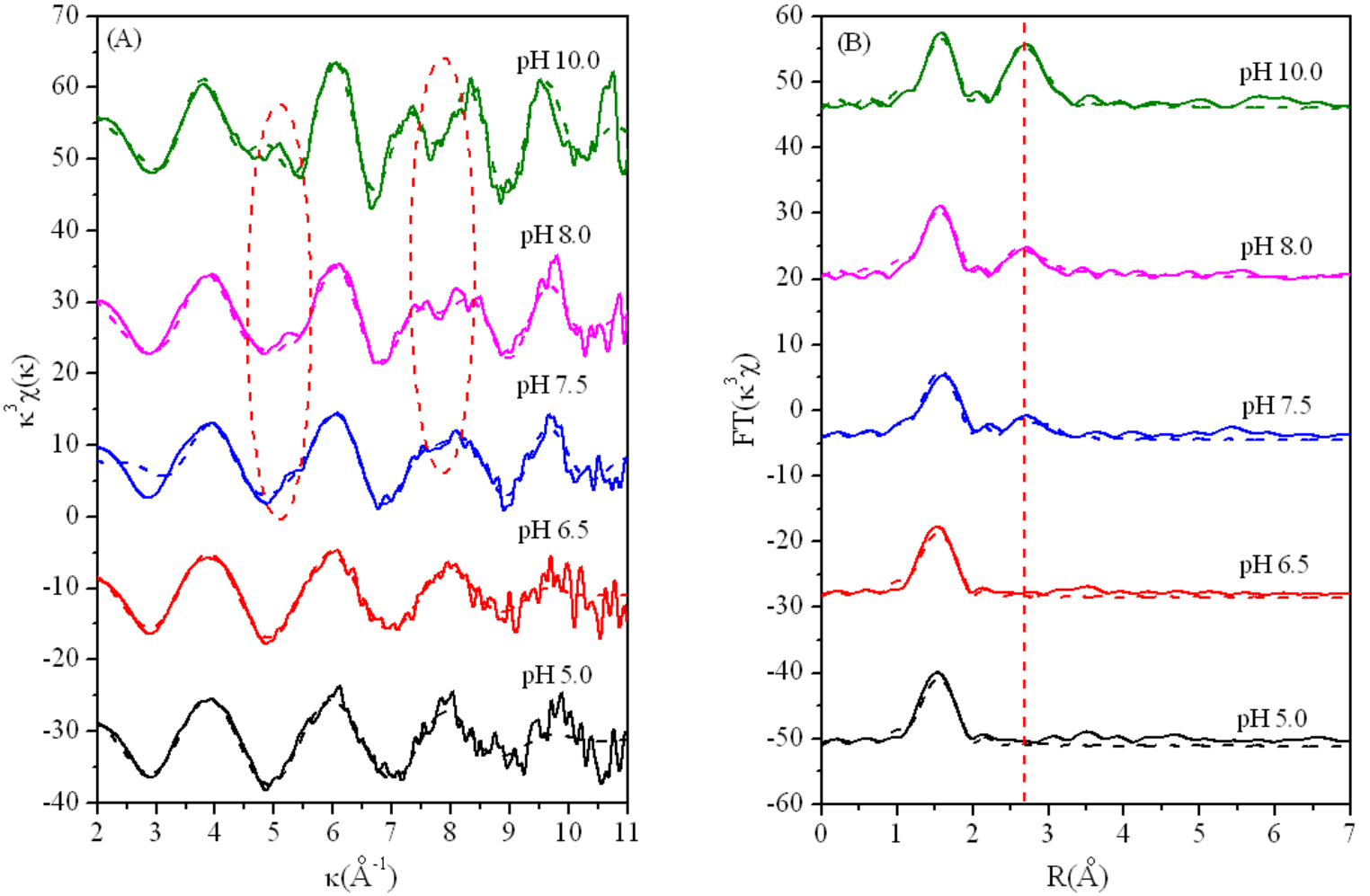
(A)
pH 10.0
pH 8.0
pH 7.5
pH 6.5
pH 5.0
κ³χ(κ)
κ(Å⁻¹)
(B)
pH 10.0
pH 8.0
pH 7.5
pH 6.5
pH 5.0
FT(κ³χ)
R(Å)

Fig. 6

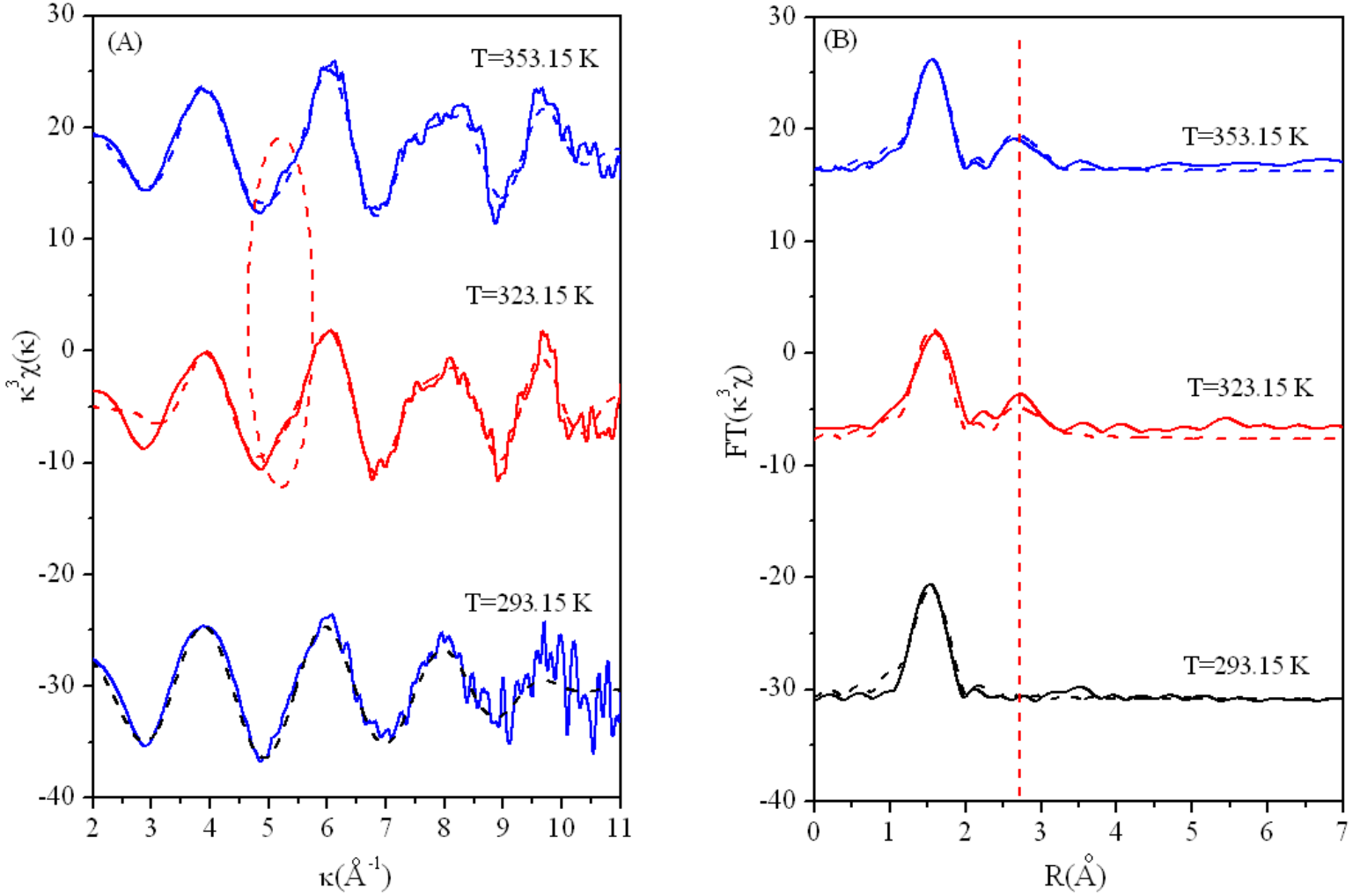
(A)
T=353.15 K
T=323.15 K
T=293.15 K
κ³χ(κ)
κ(Å⁻¹)
(B)
T=353.15 K
T=323.15 K
T=293.15 K
FT(κ³χ)
R(Å)

Fig. 7

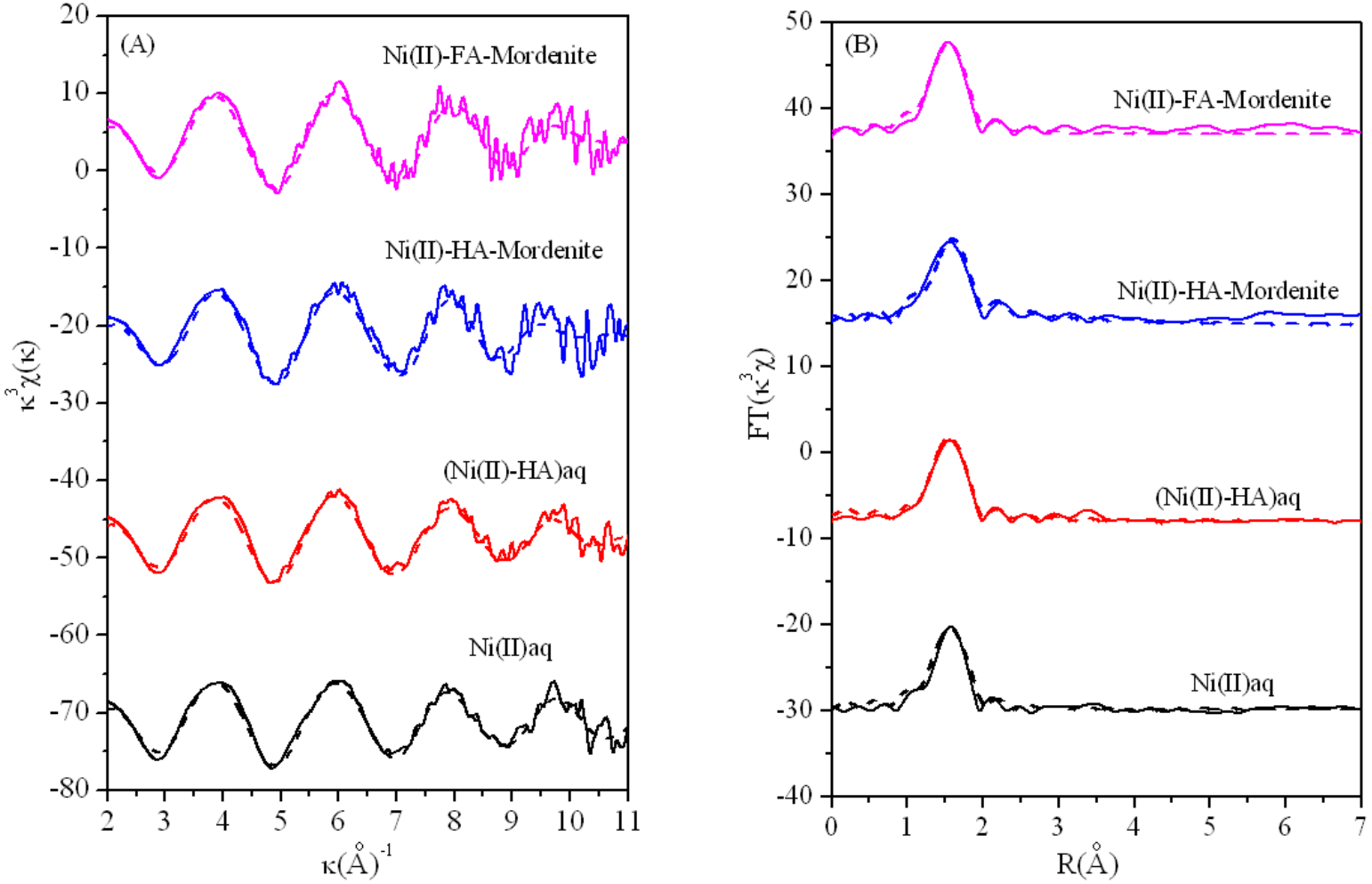
(A)
Ni(II)-FA-Mordenite
Ni(II)-HA-Mordenite
(Ni(II)-HA)aq
Ni(II)aq
κ³χ(κ)
κ(Å)⁻¹
(B)
Ni(II)-FA-Mordenite
Ni(II)-HA-Mordenite
(Ni(II)-HA)aq
Ni(II)aq
FT(κ³χ)
R(Å)

Fig. 8

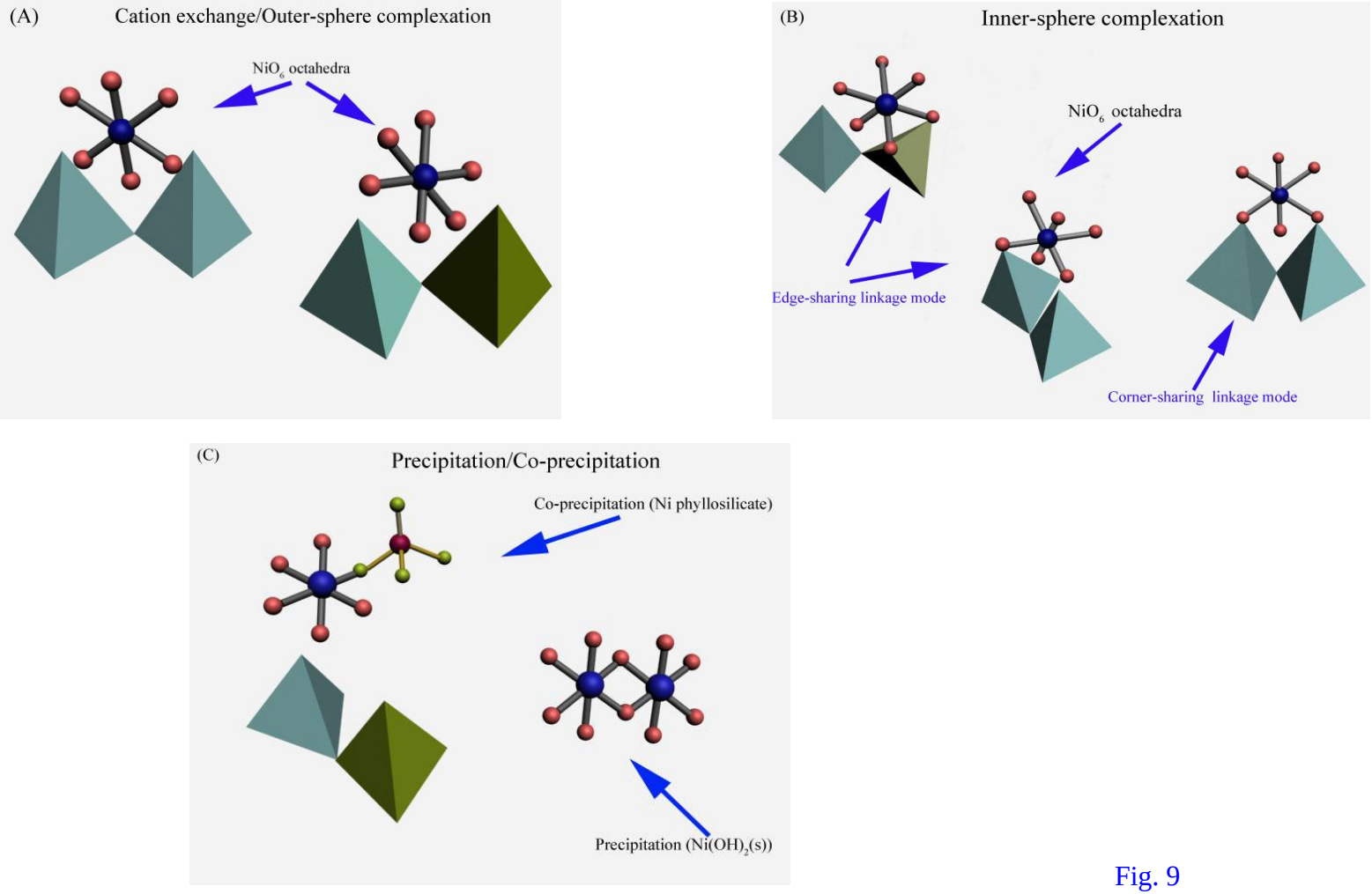
(A)
Cation exchange/Outer-sphere complexation
NiO6 octahedra
(B)
Inner-sphere complexation
NiO6 octahedra
Edge-sharing linkage mode
Corner-sharing linkage mode
(C)
Precipitation/Co-precipitation
Co-precipitation (Ni phyllosilicate)
Precipitation (Ni(OH)2(s))

Fig. 9